Mechanochemical Synthesis and Ethylenediamine Functionalization of High-Entropy ZIFs for CO_2 Adsorption and Selectivity at Elevated Temperatures

by

Md. Abu Mogira

A thesis submitted to the Graduate Faculty of
Auburn University
in partial fulfillment of the
requirements for the Degree of
Master of Science

Auburn, Alabama
April 16, 2026

Keywords: Mechanochemical synthesis; High-entropy ZIF; Amine functionalization; CO_2 adsorption; High-temperature CO_2 selectivity.

Approved by

Tae-Sik, Oh, Chair, Associate Professor, Department of Chemical Engineering
Xinyu, Zhang, Professor, Department of Chemical Engineering
Zhihua, Jiang, Associate Professor, Department of Chemical Engineering

Abstract

The development of efficient adsorbent materials for carbon dioxide (CO_2) capture is essential for reducing greenhouse gas emissions. In this study, high-entropy zeolitic imidazolate frameworks (HE-ZIFs) were synthesized via a mechanochemical ball-milling approach, providing a solvent-free and scalable route. ZIF-8 (Z8) and bimetallic ZIF (BZ) were also prepared for comparison. The materials were functionalized with ethylenediamine (EDA) at different loadings (15, 30, and 45 wt%) to enhance CO_2 adsorption and selectivity. Structural and textural analyses confirmed that moderate amine loading improves performance, while excessive loading leads to pore blockage. CO_2 adsorption results showed enhanced uptake due to combined physisorption and chemisorption effects, with HZ-15EDA exhibiting the highest capacity (~0.81 mmol g^{-1}). Selectivity analysis using mass spectrometry at 20 °C demonstrated superior CO_2 removal (~69%) for HZ-15EDA, while elevated temperature (100 °C) resulted in reduced performance due to the exothermic nature of adsorption, though amine-functionalized samples maintained relatively high selectivity. Cyclic stability tests indicated good regenerability with minimal performance loss. Overall, mechanochemically synthesized HE-ZIFs with optimized amine functionalization show strong potential for efficient CO_2 capture, particularly under elevated temperature conditions.

Acknowledgments

I would like to express my sincere gratitude to my advisor, Dr. Tae-Sik Oh, Associate Professor, Department of Chemical Engineering, for his continuous guidance, support, and encouragement throughout my research. His insights and expertise have been invaluable in shaping this work and my development as a researcher.

I am also deeply thankful to my committee members, Dr. Xinyu Zhang, Professor, Department of Chemical Engineering, and Dr. Zhihua Jiang, Associate Professor, Department of Chemical Engineering, for their valuable feedback, constructive suggestions, and time dedicated to reviewing my work.

I would like to acknowledge my labmates, Morteza Taghavi and Pritam Vitthalrao Dhawale, for their support, helpful discussions, and collaborative environment in the lab.

My sincere appreciation goes to my friends, Amad Hussen and Syed Readwan Ahmed, for their encouragement, companionship, and support throughout this journey. I am also grateful to my seniors, Shoumik Sadaf, Tanmay Rahman and Jannatul Ferdous Nipa for their guidance and advice during my academic journey.

Finally, I would like to express my deepest gratitude to my parents and siblings for their unconditional love, constant support, and sacrifices. Their encouragement has been the foundation of all my achievements.

Table of Contents

List of Figures

List Of Tables

List of Abbreviations

BET - Brunauer-Emmett-Teller

BPR - Ball-to-Powder Ratio

BZ - Bimetallic ZIF

EDA - Ethylenediamine

HZ - High-Entropy ZIF

LAG - Liquid-Assisted Grinding

MOF - Metal-Organic Framework

MS - Mass Spectrometry

SOD - Sodalite Topology

STP - Standard Temperature and Pressure

ZIF - Zeolitic Imidazolate Framework

Z8 - ZIF-8

XRD - X-ray Diffraction

Chapter 1 - Introduction

1.1 Background and Motivation

The continuous increase in atmospheric carbon dioxide (CO_2) concentration, primarily driven by fossil fuel combustion and industrial activities, has become a major contributor to global climate change[1,2]. Global CO_2 emissions have reached approximately 36-37 gigatons per year, with significant contributions from power generation, industrial processes such as cement and steel production, and transportation sectors [2–4]. This rise in greenhouse gas concentration has led to an increase in global temperature of about 1.1-1.3 °C above pre-industrial levels, resulting in environmental challenges such as extreme weather events and sea-level rise [5–7]. These concerns highlight the urgent need for effective carbon capture technologies.

Conventional carbon capture methods, particularly chemical absorption using aqueous amine solutions, are widely used in industry due to their high efficiency [8–10]. However, they suffer from key limitations including high energy consumption for regeneration, equipment corrosion, and solvent degradation, which reduce process sustainability and increase operational costs [8,9,11]. As a result, alternative approaches with improved energy efficiency and stability are actively being explored. Among these, adsorption-based CO_2 capture using porous solid materials has emerged as a promising alternative due to its lower energy requirements, operational flexibility, and potential for cyclic use [12–14]. The effectiveness of adsorption systems largely depends on the properties of the adsorbent, such as surface area, pore structure, and chemical functionality [13–16].

In this context, metal-organic frameworks (MOFs) have attracted significant attention due to their high surface area, tunable pore structures, and adjustable chemical composition, enabling

selective gas adsorption [17–20]. A subclass known as zeolitic imidazolate frameworks (ZIFs) offers additional advantages, combining the tunability of MOFs with enhanced thermal and chemical stability arising from their zeolite-like structure [21–23]. Among these materials, ZIF-8 has been extensively studied due to its well-defined microporous structure and ease of synthesis. However, ZIF-8 exhibits relatively weak interactions with CO_2, which can limit its adsorption performance, particularly at elevated temperatures [24–26]. To improve performance, several modification strategies have been explored, including metal substitution, multi-metal incorporation, and surface functionalization [27]. In particular, amine functionalization enhances CO_2 affinity through strong acid-base interactions, although it often increases regeneration energy requirements [27,28]. More recently, multi-metal and high-entropy framework materials have emerged as promising candidates, offering increased structural diversity and the potential for improved adsorption performance through synergistic effects [28–31].

Despite these advances, most studies on MOFs and ZIFs have been conducted under idealized laboratory conditions, typically involving low temperatures and pure CO_2 streams [32–34]. In contrast, real industrial flue gas conditions involve elevated temperatures (40-120 °C) and complex gas mixtures containing CO_2, N_2, water vapor, and trace impurities [35]. Under such conditions, adsorption performance is significantly affected by temperature and competitive adsorption, yet these factors remain insufficiently explored for many ZIF-based systems. Therefore, there is a clear need to develop advanced adsorbent materials that can maintain high performance under realistic operating conditions. In this regard, modified ZIF-based materials, particularly those incorporating multiple metal components and functional groups, represent a promising direction for improving CO_2 capture technologies.

1.2 Adsorption-Based CO_2 Capture and Role of MOFs and ZIFs

Carbon capture technologies can be broadly classified into absorption, adsorption, membrane separation, and cryogenic processes [36,37]. Among these, chemical absorption using liquid solvents is the most mature and widely applied method; however, it is associated with high energy consumption, corrosion, solvent degradation and environmental concerns. In contrast, adsorption-based CO_2 capture using porous solid materials has emerged as a promising alternative due to its lower energy requirement for regeneration, operational simplicity, and suitability for cyclic adsorption-desorption processes. These advantages make adsorption an attractive option for next-generation carbon capture systems. In this context, metal-organic frameworks (MOFs) have gained significant attention as advanced porous materials for gas adsorption and separation. MOFs are crystalline materials composed of metal ions or clusters coordinated with organic linkers to form three-dimensional network structures [38]. Their key advantages include exceptionally high surface area, tunable pore size distribution, and adjustable chemical composition, which enable selective adsorption of gas molecules based on size and interaction with the framework.

Among the various MOF families, zeolitic imidazolate frameworks (ZIFs) have attracted particular interest due to their enhanced thermal and chemical stability [39]. ZIFs are formed by the coordination of transition metal ions such as Zn^{2+} or Co^{2+} with imidazolate-based linkers, resulting in structures that closely resemble the topology of conventional zeolites [40–42]. ZIF-8 is one of the most extensively studied ZIF materials due to its high porosity, higher stability, SOD topology, and relatively simple synthesis. It has been widely investigated for applications such as gas storage and separation, photocatalysis, sensing and wastewater treatment [43–48]. Various modification strategies have been explored to enhance its adsorption performance. Among these, amine functionalization has shown improved CO_2 affinity [49]. More recently, the development

of multi-metal and high-entropy framework materials has emerged as a promising approach for higher catalytic activity, tunable adsorption, and defect-rich active sites compared with traditional single-metal ZIFs [50–55].

1.3 Research Gap

Although metal-organic frameworks (MOFs) and zeolitic imidazolate frameworks (ZIFs) have been extensively studied for CO_2 adsorption and separation, several limitations remain in translating their performance to practical applications. A large portion of existing studies has focused on single-metal ZIF systems like ZIF-8 and ZIF-67. Although various modification approaches have been explored, research on high-entropy ZIF systems remains limited. Most existing studies focus on catalytic applications and aromatic sulfur removal, whereas systematic evaluation of CO_2 capture performance is still lacking [50–55].

Industrial flue gas involves elevated temperatures (approximately 40-120 °C) and multicomponent gas mixtures containing CO_2, N_2, CH_4 water vapor, and other impurities [34,56–59]. Under such conditions, adsorption performance is strongly affected by temperature and competitive adsorption, which can significantly influence both capacity and selectivity. Furthermore, while various synthesis methods have been reported for MOFs and ZIFs, many conventional approaches rely on solvothermal or hydrothermal processes that require large amounts of solvent and long reaction times [60–63]. In comparison, mechanochemical synthesis offers a greener and more scalable alternative; however, its application in developing advanced high-entropy ZIF systems remains underexplored [56,64]. Single-metal ZIFs often experience a decline in adsorption performance after repeated regeneration cycles, particularly under humid or

reactive conditions, due to framework decomposition, structural transitions, and loss or blockage of active sites [65–67].

Overall, there remains a lack of comprehensive understanding regarding the combined effects of multi-metal incorporation, functionalization, synthesis methods, and operating conditions on CO_2 adsorption performance. Therefore, there is a need to develop high-entropy ZIFs synthesized via mechanochemical methods, to achieve improved adsorption capacity, selectivity, and stability under realistic operating conditions, including high-temperature adsorption behavior, temperature-dependent CO_2 selectivity, comparison with single and bimetallic ZIFs, and cyclic regeneration efficiency.

1.4 Objectives and Scope of This Work

The primary objective of this study is to investigate the synthesis, modification, and performance of amine-functionalized high-entropy zeolitic imidazolate frameworks (HE-ZIFs) for CO_2 capture applications. The specific objectives of this work are:

1.4.1 Objectives:

- Synthesize high-entropy ZIF (HE-ZIF) materials using a mechanochemical ball-milling approach with multiple metal species in equimolar ratios.
- Functionalize the synthesized materials with ethylenediamine (EDA) at different loadings to enhance CO_2 adsorption affinity.
- Characterize the structural and textural properties of the materials using techniques such as X-ray diffraction (XRD) and BET surface area analysis.
- Evaluate CO_2 adsorption capacity using gas adsorption measurements.

- Investigate CO_2 selectivity using mixed-gas systems (CO_2/CH_4/He) analyzed by mass spectrometry.
- Study the effect of amine loading and operating temperature on adsorption performance (20 °C and 100 °C).
- Assess the regeneration and cyclic stability of the materials through multiple adsorption-desorption cycles.
- Compare the performance of HE-ZIF materials with conventional ZIF-8 and bimetallic ZIF systems.

1.4.2 Scope of the Study:

This work focuses on the development and evaluation of amine-functionalized HE-ZIF materials synthesized via a green mechanochemical route. The study aims to understand how multi-metal incorporation, functionalization, and operating conditions influence CO_2 adsorption capacity, selectivity, and stability, with an emphasis on performance under elevated temperature conditions relevant to practical applications.

Chapter 2 - Literature Review

2.1 CO_2 Capture Technologies

Carbon capture technologies are generally classified into absorption, adsorption, membrane separation, and cryogenic processes, each differing in mechanism, energy requirement, and applicability to industrial systems. Chemical absorption, particularly using aqueous amine solvents such as monoethanolamine (MEA), is the most established technology for post-combustion CO_2 capture. Industrial systems employing MEA can achieve capture efficiencies of 85-95%, making them suitable for large-scale applications such as power plants [10,37,68,69]. However, this process is associated with a significant energy penalty during solvent regeneration, typically in the range of 3-4 GJ per ton of CO_2, which accounts for a substantial fraction of the total plant energy consumption [37]. Additional challenges include solvent degradation in the presence of oxygen and impurities, equipment corrosion, and high operational costs, all of which limit long-term process efficiency [70].

Adsorption-based CO_2 capture relies on porous solid materials that interact with gas molecules through physical or chemical forces. Common absorbents include activated carbons, zeolites, Mesoporous silica, Porous organic polymers and metal-organic frameworks (MOFs) [71]. Compared to absorption, adsorption processes generally require lower regeneration energy (often <2 GJ per ton of CO_2) and offer advantages such as rapid adsorption kinetics, modular operation, and easier cycling through pressure or temperature swing processes. Zeolites exhibit high CO_2 uptake due to strong electrostatic interactions but are sensitive to moisture, while activated carbons provide good stability with moderate adsorption capacity [71,72]. More recently, MOF-303,

HKUST-1 aerogels, and defect-engineered MOF-808 have demonstrated high CO_2 adsorption capacities (5–8 mmol g^{-1}) at 1 bar and near-ambient temperature [73–75].

Membrane-based separation has been explored as an energy-efficient alternative due to its compact design, continuous operation, and relatively low energy consumption. Gas separation membranes operate based on differences in permeability and diffusivity of gas molecules. Polymeric membranes typically exhibit CO_2 permeabilities in the range of 100-1000 Barrer, with selectivity values varying depending on material composition [76–78]. However, membrane systems are often constrained by the trade-off between permeability and selectivity, as described by the Robeson upper bound [78]. In addition, membrane performance can be significantly affected by impurities, pressure fluctuations, and elevated temperatures, which are common in industrial flue gas streams [79].

Cryogenic separation is based on the condensation or desublimation of CO_2 at low temperatures, enabling the production of high-purity CO_2 streams [80,81]. This approach is particularly effective for gas streams with high CO_2 concentrations. However, the process requires substantial energy input for refrigeration, making it less suitable for dilute CO_2 streams such as flue gas, where CO_2 concentrations are typically below 15% [82].

2.2 Adsorbent Materials for CO_2 Capture

A wide range of porous materials has been investigated for adsorption-based CO_2 capture, including activated carbons, zeolites, silica-based materials, amine-functionalized adsorbents, and metal-organic frameworks (MOFs). The effectiveness of these materials depends on key properties such as surface area, pore structure, chemical functionality, and selectivity toward CO_2, particularly in the presence of competing gases.

Activated carbons are widely used due to their low cost, high thermal stability, and resistance to moisture. These materials typically exhibit surface areas in the range of 500-2000 m^2g^{-1} and CO_2 adsorption capacities of approximately 1-3 mmol g^{-1} at ambient conditions [83,84]. Their adsorption mechanism is primarily based on physisorption, which enables fast kinetics and easy regeneration with relatively low energy input. However, due to the absence of specific functional groups, activated carbons generally exhibit lower selectivity toward CO_2 compared to other adsorbents, especially in mixed-gas environments [85].

Zeolites, such as 13X and 5A, are crystalline aluminosilicate materials with well-defined microporous structures and strong electrostatic fields [86][87]. These materials can achieve CO_2 adsorption capacities of 3-5 mmol g^{-1} at 25 °C, along with high selectivity resulting from strong interactions between CO_2 molecules and cationic sites within the framework[87]. Compared to activated carbons, zeolites provide higher selectivity and stronger adsorption interactions, but they are highly sensitive to moisture, as water molecules preferentially occupy adsorption sites and significantly reduce CO_2 uptake under humid conditions [87]. This limitation restricts their applicability in real flue gas environments.

Silica-based materials, including mesoporous structures such as SBA-15 and MCM-41, offer high surface area and tunable pore sizes, but their intrinsic CO_2 adsorption capacity is relatively low due to weak interactions with CO_2 molecules [88,89]. To improve performance, these materials are often functionalized with amine groups, which enhances adsorption capacity to approximately 2-4 mmol g^{-1} [90–92]. While functionalized silica exhibits improved selectivity compared to unmodified silica, the introduction of amine groups often results in higher regeneration energy requirements, similar to other chemisorption-based systems[90,91].

Amine-functionalized adsorbents, including grafted porous materials and polymer-supported amines, have been extensively studied due to their high CO_2 selectivity and strong adsorption affinity[93,94]. These materials capture CO_2 primarily through chemisorption via carbamate formation, enabling effective adsorption even at low CO_2 partial pressures. Reported CO_2 capacities typically range from 3-6 mmol g^{-1}, often exceeding those of activated carbons and comparable to or higher than zeolites under certain conditions[93,95]. However, the strong interaction between CO_2 and amine groups leads to higher energy requirements for regeneration, and these materials may also suffer from oxidative degradation and reduced stability over repeated adsorption-desorption cycles [96].

Among advanced porous materials, metal-organic frameworks (MOFs) have attracted significant attention due to their exceptionally high surface, tunable pore structures, and adjustable chemical functionality[97–99]. These properties enable MOFs to achieve CO_2 adsorption capacities typically in the range of 2-6 mmol g^{-1} under ambient conditions, with the potential for enhanced selectivity through functionalization or structural design [97,98,100]. Compared to conventional adsorbents, MOFs offer a unique advantage in terms of tunability and design flexibility, allowing precise control over adsorption behavior. However, certain MOFs exhibit limited stability in the presence of moisture or under harsh operating conditions, which remains a key challenge for their practical application.

2.3 MOFs and ZIFs for CO_2 Adsorption

Metal-organic frameworks (MOFs) are a class of crystalline porous materials composed of metal ions or metal clusters coordinated with organic linkers to form extended three-dimensional network structures. This coordination results in highly ordered frameworks with well-defined pore systems and exceptionally high surface areas, often exceeding 3000 m^2g^{-1}[18,101]. The structural diversity of MOFs arises from the wide range of possible combinations between metal nodes and organic linkers, allowing precise control over pore size, shape, and surface functionality.

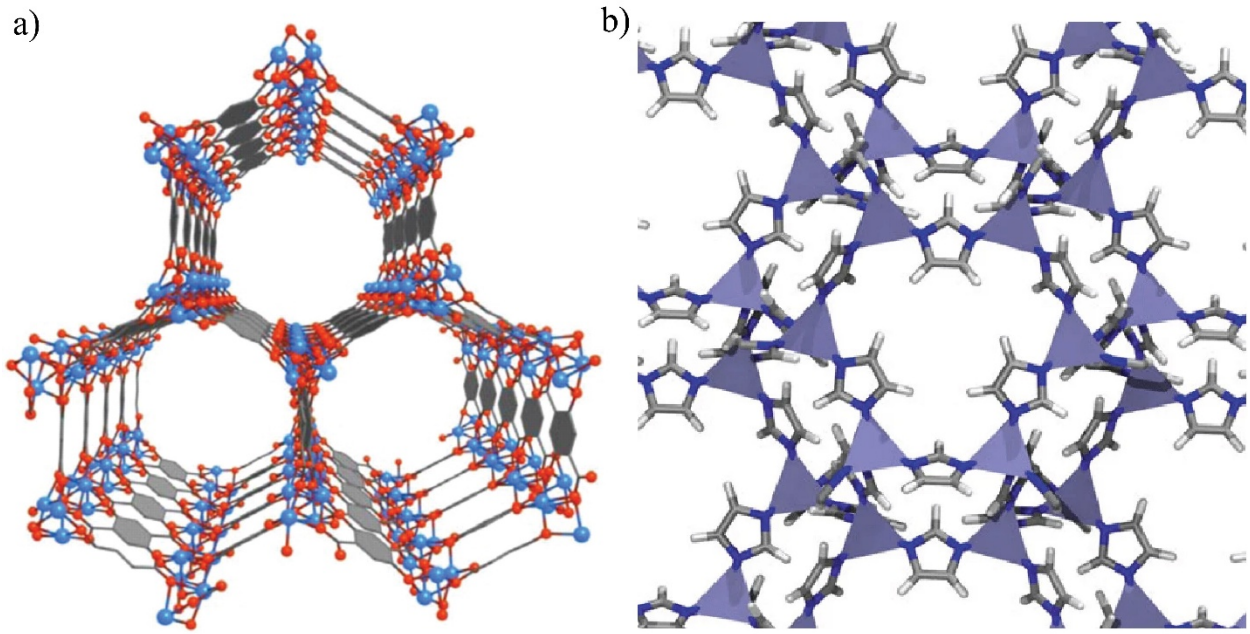

Figure 2.1 Structural representation of (a) Mg-MOF-74 and (b) ZIF-8. Mg-MOF-74 consists of metal–oxide chains connected by organic linkers with open metal sites, while ZIF-8 is formed by metal–imidazolate coordination (~145° bond angle), creating a porous cage like structure.

The fundamental structure of MOFs is illustrated in Figure 2.1(a), where metal nodes are connected by organic ligands to form an extended porous network with accessible channels and cavities suitable for gas adsorption. These structural characteristics enable MOFs to selectively adsorb gas molecules based on molecular size, polarity, and specific interactions with the

framework. As a result, MOFs have been widely investigated for CO_2 capture, with reported adsorption capacities typically ranging from 2 to 6 mmol g^{-1} under ambient conditions, depending on their composition and functionalization [100,102]. Several advantages make MOFs attractive for CO_2 adsorption applications. Their high surface area provides abundant adsorption sites, while their tunable pore structure allows optimization for selective gas separation. In addition, the incorporation of functional groups into the framework can enhance interactions with CO_2 molecules, improving adsorption capacity and selectivity [58]. However, despite these advantages, some MOFs exhibit limited thermal and chemical stability, particularly in the presence of moisture, which can restrict their practical application in industrial environments.

Within the broader MOF family, zeolitic imidazolate frameworks (ZIFs) represent a unique subclass that combines the structural tunability of MOFs with the robustness of traditional zeolites. ZIFs are formed by the coordination of transition metal ions, such as Zn^{2+} or Co^{2+}, with imidazolate-based linkers, resulting in frameworks that closely resemble zeolite topologies [102,103]. As shown in Figure 2.1(b), ZIF structures exhibit a characteristic cage-like architecture connected through narrow pore windows, arising from the metal-imidazolate-metal bond angle of approximately 145°, which is analogous to the Si-O-Si bond angle in zeolites [102–104].

The zeolite-like structure of ZIFs imparts several important advantages. In particular, ZIFs exhibit enhanced thermal and chemical stability compared to many conventional MOFs, making them more suitable for applications involving variable temperatures and harsh operating conditions. For example, ZIF-8 has demonstrated stability at temperatures exceeding 400 °C and resistance to degradation in aqueous environments, which is critical for CO_2 capture from flue gas streams containing moisture [105,106]. ZIF materials have also shown promising performance for

CO_2 adsorption due to their microporous structure and favorable pore size distribution, which facilitate selective adsorption of CO_2 molecules. However, similar to other MOFs, the interaction between CO_2 and the framework in many ZIFs is primarily governed by physisorption, leading to moderate adsorption capacity and selectivity, particularly at elevated temperatures.

Despite these limitations, ZIFs remain highly promising for CO_2 capture due to their structural stability, tunability, and compatibility with various modification strategies. Approaches such as metal substitution, multi-metal incorporation, and surface functionalization can be used to enhance adsorption performance and tailor material properties. These features make ZIF-based materials, especially advanced systems such as multi-metal and high-entropy ZIFs, attractive candidates for further development in adsorption-based carbon capture technologies.

2.4 CO_2 Adsorption Mechanism in ZIFs

The adsorption of CO_2 in zeolitic imidazolate frameworks (ZIFs) is predominantly governed by physisorption mechanisms, particularly in non-functionalized systems such as ZIF-8. In this process, gas molecules are adsorbed onto the internal surfaces of porous materials through relatively weak intermolecular forces, including van der Waals interactions and electrostatic forces, without the formation of strong chemical bonds [107–109]. This mechanism is

characterized by low adsorption enthalpy, rapid adsorption-desorption kinetics, and good reversibility, making it suitable for cyclic CO_2 capture processes.

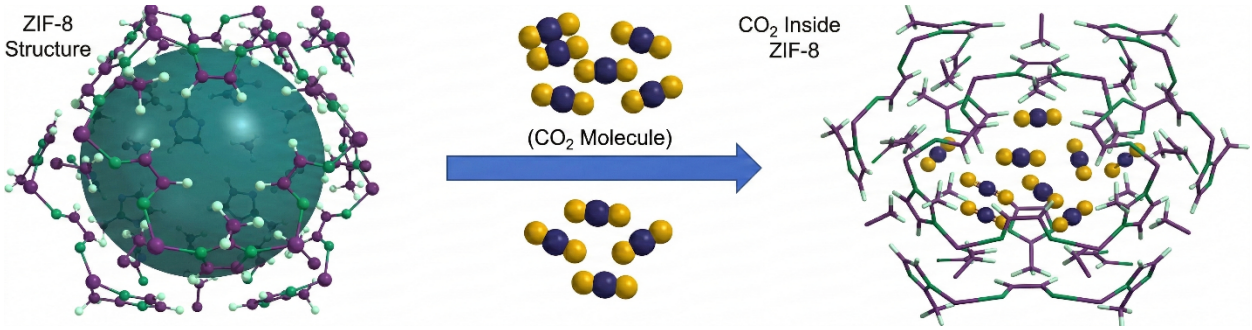

Figure 2.2 Schematic of CO_2 adsorption in ZIF-8, illustrating diffusion into pore cages and adsorption via weak van der Waals interactions.

A schematic representation of CO_2 adsorption within porous frameworks is shown in Figure 2.2, where CO_2 molecules are confined within the pore network and interact with the internal surface of the material. The efficiency of this process is strongly influenced by the pore architecture, particularly in ZIF materials with well-defined crystalline structures.

ZIF-8, one of the most widely studied ZIF materials, exhibits a sodalite (SOD) topology, consisting of large internal cavities (cages) interconnected by narrow pore openings (windows). The cage diameter of ZIF-8 is approximately 11.6 Å, while the window aperture is about 3.4 Å [59,110,111]. In comparison, the kinetic diameter of a CO_2 molecule is approximately 3.3 Å, which is very close to the window size [112,113]. This size compatibility allows CO_2 molecules to diffuse through the pore openings and be adsorbed within the cages, as illustrated in Figure 2.2. In contrast, slightly larger or less interactive molecules may experience restricted diffusion, contributing to selective adsorption.

The zeolite-like structure of ZIFs, particularly their SOD topology, plays a crucial role in enhancing CO_2 capture performance [114]. The narrow pore windows act as molecular sieves,

allowing selective access based on molecular size, while the larger internal cages provide sufficient space for adsorption. This combination of size-selective diffusion and pore confinement enhances the interaction between CO_2 molecules and the framework, even though the overall interaction remains primarily physical in nature [111]. The pore confinement effect is especially important in microporous materials, where the proximity of pore walls increases the interaction potential between gas molecules and the adsorbent surface. In addition, the presence of metal sites within the framework can influence adsorption behavior [115,116]. Although ZIF-8 does not possess highly polar or open metal sites, modifications such as metal substitution or multi-metal incorporation can introduce regions of enhanced electrostatic interaction, potentially improving CO_2 affinity.

Despite these advantages, the physisorption mechanism is inherently sensitive to operating conditions. At elevated temperatures, the strength of van der Waals interactions decreases, resulting in reduced adsorption capacity [111]. Furthermore, in multicomponent systems, competitive adsorption may occur, where gases such as N_2or water vapor occupy available adsorption sites, affecting both capacity and selectivity. Understanding the relationship between framework structure, pore geometry, and intermolecular interactions is therefore essential for optimizing ZIF materials for CO_2 capture. These insights provide a basis for designing advanced materials with improved performance under realistic conditions.

2.5 High-Entropy ZIFs

The incorporation of multiple metal species into zeolitic imidazolate frameworks (ZIFs) has emerged as an effective strategy for tuning structural and adsorption properties. In particular, the concept of high-entropy materials, originally developed for metallic alloys, has recently been

extended to porous framework systems. Early efforts in this direction focused on bimetallic ZIF systems, in which two different metal ions (e.g., Zn^{2+} and Co^{2+}) are incorporated into the framework [117,118]. These systems have demonstrated improvements in CO_2 adsorption performance compared to single-metal ZIFs, primarily due to modifications in local electronic structure, pore environment, and metal-ligand interactions [117–119]. High-entropy materials typically consist of five or more elements distributed within a single crystalline lattice, where the configurational entropy plays a key role in stabilizing the structure. In high-entropy ZIFs (HE-ZIFs), multiple metal ions are incorporated into a single framework, forming a uniform multi-metal distribution, as illustrated in Figure 2.3.

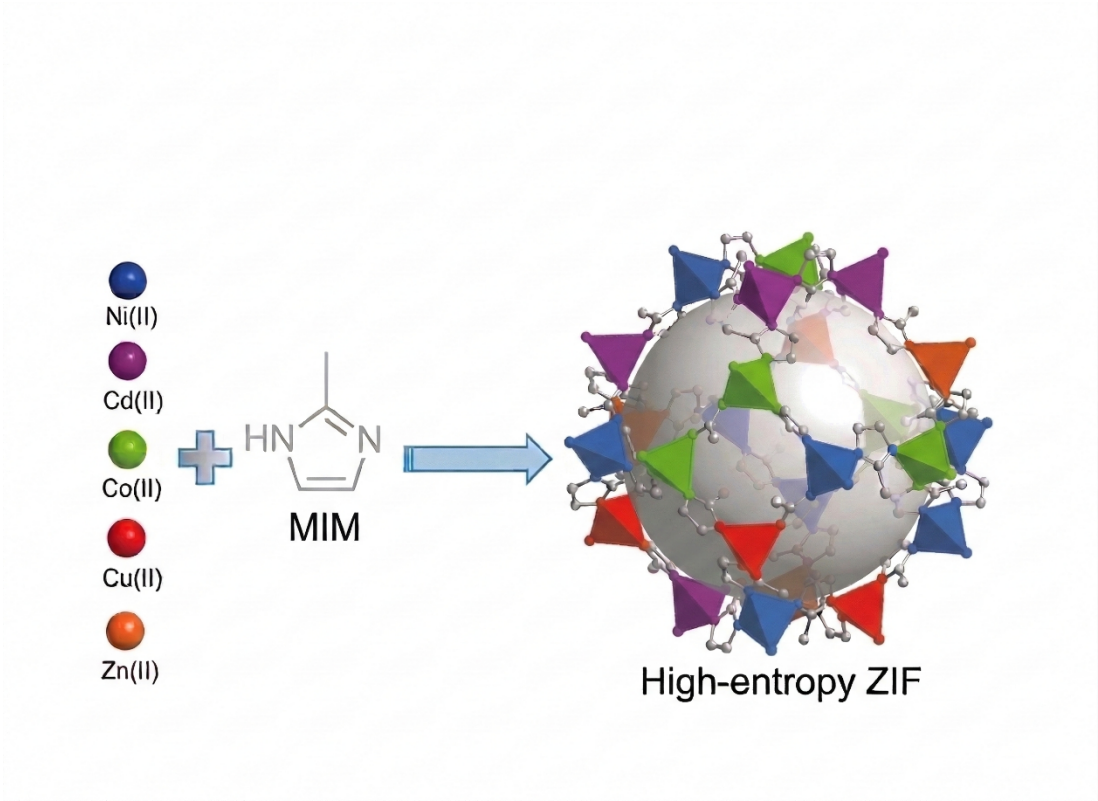

Figure 2.3 Schematic representation of high-entropy ZIF (HE-ZIF) formation, illustrating the incorporation and uniform distribution of multiple metal ions (Ni^{2+}, Cd^{2+}, Co^{2+}, Cu^{2+}, and Zn^{2+}) coordinated with 2-methylimidazolate linkers.

The configurational entropy associated with such systems can be expressed as:

$$\Delta S_{config} = -R \sum_i x_i \ln x_i$$

where x_i represents the mole fraction of each metal component. As the number of metal species increases, configurational entropy increases, promoting the formation of a stable single-phase structure [120,121].

The thermodynamic stability of high-entropy ZIFs can be further understood using the Gibbs free energy relationship:

$$\Delta G = \Delta H - T\Delta S$$

An increase in configurational entropy (ΔS_{config}) contributes to lowering the Gibbs free energy of the system, thereby favoring the formation of a thermodynamically stable framework. This entropy-driven stabilization is particularly important in multi-metal systems, where it helps suppress phase separation and maintain structural integrity [121–123].

In addition to improved stability, high-entropy ZIFs offer several advantages over conventional and bimetallic systems. The presence of multiple metal species introduces structural and chemical heterogeneity, which can enhance interactions between CO_2 molecules and the framework [123]. Furthermore, synergistic effects between different metal centers can create a diverse range of adsorption sites with varying binding strengths, potentially improving both adsorption capacity and selectivity [123–125]. The incorporation of multiple metals can also induce lattice distortion and modification of pore environments, influencing diffusion behavior and adsorption characteristics [124,125].

Another important advantage of high-entropy ZIFs is their potential for improved thermal stability and resistance to harsh operating conditions. The entropy-driven stabilization mechanism can enhance resistance to structural degradation at elevated temperatures, which is critical for applications involving flue gas streams [126,127]. This makes HE-ZIFs particularly attractive for high-temperature CO_2 capture, where conventional ZIF materials often exhibit reduced performance.

Despite these promising characteristics, research on high-entropy ZIFs remains relatively limited[124,125]. Most reported studies have focused on the successful synthesis and structural characterization of multi-metal frameworks, demonstrating uniform metal distribution and stable crystalline structures. Some studies have reported enhanced surface area, modified pore structures, and improved gas adsorption performance compared to single-metal systems [124,125]. However, systematic investigations into CO_2 adsorption capacity, selectivity, and stability under realistic conditions are still scarce. In particular, there is a lack of studies evaluating the performance of high-entropy ZIFs at elevated temperatures and in multicomponent gas systems, where competitive adsorption and thermal effects significantly influence performance. As a result, the full potential of HE-ZIF materials for practical CO_2 capture applications remains largely unexplored.

2.6 Amine-Functionalized Adsorbents and Chemisorption

Amine-functionalized adsorbents have been extensively investigated for CO_2 capture due to their high selectivity and strong affinity toward CO_2 molecules [128]. Unlike conventional porous materials such as ZIFs, where adsorption is primarily governed by physisorption, amine-

based systems rely on chemisorption mechanisms, involving the formation of chemical bonds between CO_2 and amine groups [129,130].

The primary mechanism of CO_2 capture in amine-functionalized materials is the formation of carbamate species through an acid-base reaction between CO_2 and primary or secondary amines. This reaction can be represented as:

$$CO_2 + 2RNH_2 \rightarrow RNHCOO^- + RNH_3^+$$

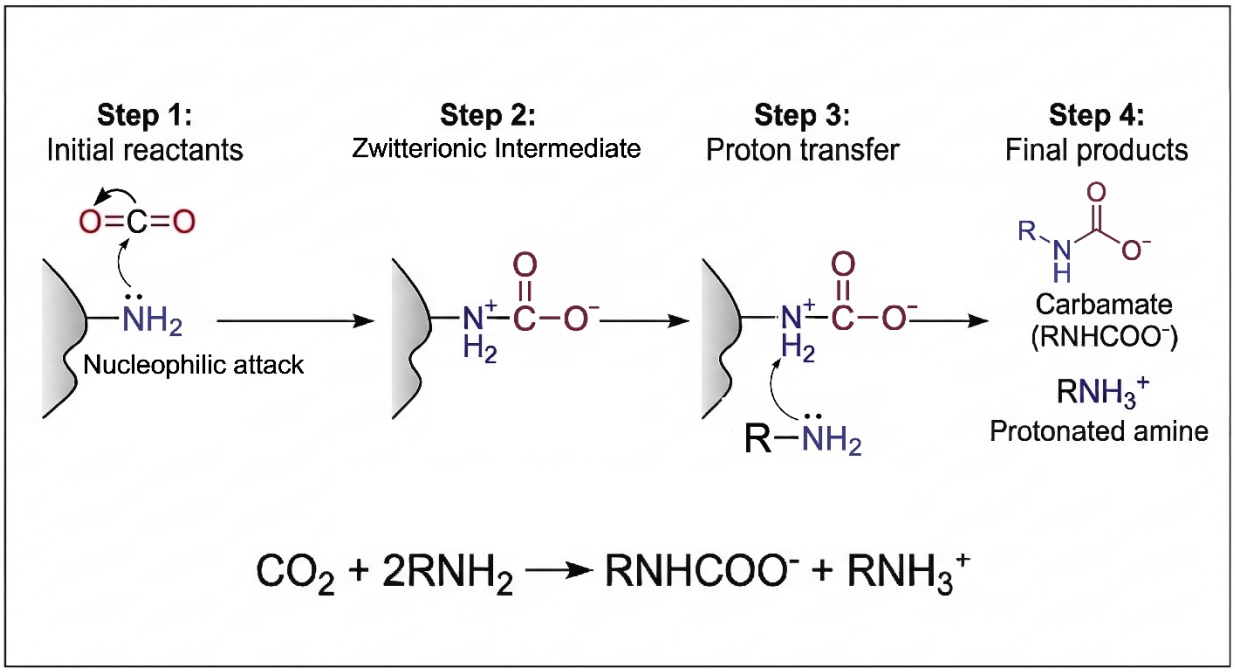

Figure 2.4 Stepwise mechanism of CO2 chemisorption on amine-functionalized adsorbents, showing nucleophilic attack, zwitterion formation, proton transfer, and formation of carbamate (RNHCOO-) and protonated amine (RNH3+).

As illustrated in Figure 2.4, CO_2 molecules react with amine groups anchored on the adsorbent surface to form carbamate ions, resulting in strong and selective adsorption. In some cases, particularly in the presence of moisture, CO_2 may also form bicarbonate species, which can further influence adsorption behavior[129–132]. This chemisorption mechanism provides several advantages for CO_2 capture. Most notably, amine-functionalized adsorbents exhibit high

selectivity toward CO_2, even in the presence of other gases such as N_2 or CH_4. The strong interaction between CO_2 and amine groups allows effective capture at low CO_2 partial pressures, making these materials particularly suitable for post-combustion applications [129,131,132]. Additionally, amine-functionalized materials can achieve relatively high adsorption capacities, often in the range of 3-6 mmol g^{-1}, depending on amine loading and material structure.

However, the strong chemical bonding associated with chemisorption also introduces certain limitations. The regeneration of amine-based adsorbents requires higher energy input compared to physisorption-based systems, as the carbamate bonds must be broken during desorption [133]. This results in increased thermal energy demand and can reduce overall process efficiency. Furthermore, amine-functionalized materials may experience degradation over repeated adsorption-desorption cycles, particularly in the presence of oxygen, moisture, or acidic impurities, which can affect long-term stability [134–137]. Despite these challenges, amine-functionalized adsorbents remain an important class of materials for CO_2 capture due to their high selectivity and strong adsorption performance. Their behavior also provides a useful contrast to physisorption-based systems such as ZIFs, highlighting the trade-off between adsorption strength and regeneration energy in the design of effective carbon capture materials.

2.7 Regeneration and Stability of ZIF Adsorbents

For practical CO_2 capture applications, the performance of an adsorbent is determined not only by its adsorption capacity and selectivity but also by its regeneration ability and long-term stability. Regeneration refers to the removal of adsorbed gas molecules from the adsorbent surface, allowing the material to be reused in repeated adsorption-desorption cycles. In industrial systems,

adsorbents operate continuously under cyclic conditions; therefore, maintaining structural integrity and consistent performance over multiple cycles is essential.

Regeneration of ZIF adsorbents is typically achieved through temperature swing adsorption (TSA) or pressure swing adsorption (PSA) processes [138]. In TSA, the material is heated to desorb CO_2, while in PSA, pressure reduction facilitates gas release. These processes rely on the reversible nature of adsorption, particularly in ZIF materials where physisorption dominates, enabling relatively efficient regeneration with lower energy requirements compared to chemisorption-based systems [139,140]. ZIF materials are known for their high thermal and chemical stability, which makes them suitable for repeated adsorption-desorption cycles. For example, ZIF-8 has been reported to maintain structural stability at temperatures exceeding 400 °C, indicating strong resistance to thermal degradation [138,139,141]. This stability allows ZIF adsorbents to retain their framework structure and adsorption performance over multiple cycles. However, adsorption capacity may decrease at elevated temperatures due to the weakening of physisorption interactions. The cyclic performance of ZIF adsorbents is generally favorable, as the reversible adsorption mechanism minimizes structural changes during operation. Several studies have demonstrated that ZIF materials can maintain a significant portion of their initial CO_2 adsorption capacity over repeated cycles [134,135,138,140]. Nevertheless, factors such as moisture exposure, impurities, and pore blockage can gradually affect performance, particularly under realistic operating conditions. Modifications to ZIF structures, including metal substitution, multi-metal incorporation, and functionalization, can influence regeneration behavior. While these modifications often enhance adsorption capacity or selectivity, they may also alter pore accessibility, adsorption strength, and thermal stability, potentially affecting regeneration efficiency.

In particular, amine-functionalized ZIF adsorbents exhibit different regeneration characteristics compared to non-functionalized systems. The strong interaction between CO_2 and amine groups, associated with chemisorption, leads to higher regeneration energy requirements due to the need to break carbamate bonds during desorption. Additionally, repeated adsorption-desorption cycles may result in gradual degradation of amine groups or loss of active sites, which can reduce long-term performance.

Chapter 3 - Experimental Methods

3.1 Materials

All chemicals used in this study were of analytical grade and used without further purification. Zinc oxide (ZnO), copper oxide (CuO), cadmium oxide (CdO), nickel acetate tetrahydrate ($Ni(OAc)_2 \cdot 4H_2O$), and cobalt acetate tetrahydrate ($Co(OAc)_2 \cdot 4H_2O$) were used as metal precursors for the synthesis of zeolitic imidazolate frameworks. The CuO and CdO used in this study were prepared by thermal decomposition of copper nitrate tetrahydrate ($Cu(NO_3)_2 \cdot 4H_2O$) and cadmium nitrate tetrahydrate ($Cd(NO_3)_2 \cdot 4H_2O$), respectively, in a furnace at 450 °C for 5 hours.

2-methylimidazole (Hmim) was used as the organic ligand for framework formation. Methanol (MeOH) was used as the solvent for liquid-assisted grinding during mechanochemical synthesis and also for washing the synthesized materials. Ethylenediamine (EDA) was used as the amine functionalization agent for post-synthetic modification of the synthesized ZIF materials. The amine functionalization was performed at different loadings to evaluate its influence on CO_2 adsorption and selectivity.

For adsorption and selectivity experiments, carbon dioxide (CO_2), methane (CH_4), and helium (He) gases with high purity were used as feed gases. These gases were supplied through mass flow controllers during the gas adsorption and selectivity measurements. Methanol were used during liquid assisted Grinding (LAG) and washing the excess ligand.

3.2 Mechanochemical Synthesis of ZIF Materials

All zeolitic imidazolate framework (ZIF) materials used in this study were synthesized using an Across International PQ-N2 planetary ball mill following a mechanochemical synthesis process. Mechanochemical synthesis was selected due to its rapid reaction kinetics, reduced solvent consumption, scalability, and scalability, and ability to synthesize at room temperature. A ball mill equipped with zirconia milling balls was used to induce the coordination reaction between metal precursors and the organic ligand through mechanical energy.

In all syntheses, liquid-assisted grinding (LAG) was employed by adding a small amount of methanol to improve the interaction between metal precursors and the organic ligand. Milling was performed at 400 rpm using 10 mm zirconia balls with a ball-to-powder ratio of 10:1. After milling, the synthesized powders were washed with methanol to remove residual reactants and then dried prior to characterization and adsorption experiments.

The synthesis procedures for the high-entropy ZIF, conventional ZIF-8, and bimetallic ZIF materials are described in the following subsections.

3.2.1 Synthesis of High-Entropy ZIF (HE-ZIF)

High-entropy zeolitic imidazolate framework (HE-ZIF) was synthesized using a mechanochemical ball-milling method with stepwise incorporation of multiple metal precursors. The composition and synthesis parameters are summarized in Table 3.1.

Table 3.1 Composition and synthesis conditions of HE-ZIF

Component Type	Chemical	Amount (g)	Mols (mol)	Milling Time (min)
Metal Source	ZnO	0.33	0.004	10
	CuO	0.32	0.004	5
	CdO	0.51	0.004	5
	$Ni(OAc)_2 \cdot 4H_2O$	1.00	0.004	5
	$Co(OAc)_2 \cdot 4H_2O$	0.99	0.004	5
Organic Linker	2-methylimidazole (Hmim)	8.21	0.1	
Solvent (LAG)	Methanol (MeOH)	0.50 mL		

Zinc oxide (ZnO), copper oxide (CuO), cadmium oxide (CdO), nickel acetate tetrahydrate ($Ni(OAc)_2 \cdot 4H_2O$), and cobalt acetate tetrahydrate ($Co(OAc)_2 \cdot 4H_2O$) were used as metal sources in equimolar amounts (0.004 mol each), resulting in a total metal content of 0.02 mol. The organic ligand, 2-methylimidazole (Hmim), was added to maintain a metal-to-ligand molar ratio of 1:5.

The synthesis was carried out in a ball mill using 10 mm zirconia milling balls in a 300 mL stainless steel canister, with a ball-to-powder ratio of 10:1. Liquid-assisted grinding (LAG) was employed by adding 0.5 mL of methanol (0.044 μL/mg) to facilitate coordination between the metal ions and the organic ligand. Initially, ZnO and Hmim were milled at 400 rpm for 10 minutes. The remaining metal precursors (CuO, CdO, $Ni(OA_C)_2 \cdot 4H_2O$, and $Co(OA_C)_2 \cdot 4H_2O$) were then

added sequentially, with each addition followed by 5 minutes of milling under identical conditions. After incorporation of the final metal precursor, an additional 10 minutes of milling was performed to complete the synthesis.

To evaluate the effect of milling duration on the formation and crystallinity of HE-ZIF, post-milling was applied after the initial synthesis step. As presented in Table 3.2, post-milling times of 10, 30, and 60 minutes were used, resulting in total milling durations of 40, 60, and 90 minutes, respectively. The resulting samples were labeled as HZ-40, HZ-60, and HZ-90 based on their total milling time.

Table 3.2 Post-milling and total milling times of HE-ZIF samples

Sample Name	Initial Milling (min)	Post-Milling (min)	Total Time (min)
HZ-40	30	10	40
HZ-60	30	30	60
HZ-90	30	60	90

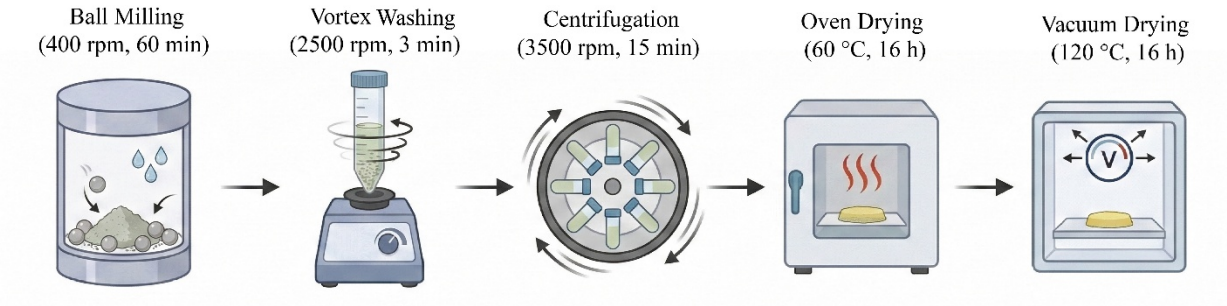

Figure 3.1 Schematic of HE-ZIF synthesis and processing steps.

A schematic representation of the synthesis and post-processing steps is shown in Figure 3.1, illustrating the sequential processes involved, including ball milling, vortex washing, centrifugation, and drying.

Following synthesis, the obtained powder was washed with methanol to remove unreacted precursors and residual ligand. The sample was dispersed in 30 mL of methanol and vortex-washed at 2500 rpm for 3 minutes, followed by centrifugation at 3500 rpm for 15 minutes. This washing cycle was repeated three times. The collected precipitate was then dried in an oven at 60 °C for approximately 16 hours, followed by vacuum drying at 120 °C for 16 hours to remove residual solvent and activate the porous structure.

3.2.2 Synthesis of ZIF-8

ZIF-8 was synthesized using zinc oxide (ZnO) as the metal precursor and 2-methylimidazole (Hmim) as the organic ligand, maintaining a metal-to-ligand molar ratio of 1:2. The reactants were mixed with 0.5 mL methanol to facilitate liquid-assisted grinding and placed

in a 300 mL stainless steel canister containing 10 mm zirconia milling balls with a ball-to-powder ratio of 10:1. The mixture was milled at 400 rpm for 60 minutes to promote coordination between zinc ions and the ligand, resulting in the formation of the ZIF-8 framework.

Following synthesis, the obtained powder was washed with methanol to remove unreacted precursors and residual ligand. The sample was dispersed in 30 mL of methanol, vortex-mixed at 2500 rpm for 3 minutes, and centrifuged at 3500 rpm for 15 minutes. This washing cycle was repeated three times. The collected precipitate was dried in an oven at 60 °C for approximately 16 hours, followed by vacuum drying at 120 °C for 16 hours to remove residual solvent and activate the porous structure.

3.2.3 Synthesis of Bimetallic ZIF

A bimetallic ZIF was synthesized using zinc oxide (ZnO) and cobalt acetate tetrahydrate ($Co(OA_C)_2 \cdot 4H_2O$) as metal precursors in equimolar amounts (0.02 mol each). The metal precursors were combined with 2-methylimidazole (Hmim) as the organic ligand, maintaining a metal-to-ligand molar ratio of 1:4.

The reactant mixture was placed in a 300 mL stainless steel canister containing 10 mm zirconia milling balls with a ball-to-powder ratio of 10:1. Liquid-assisted grinding was performed by adding 0.5 mL methanol. The mixture was milled at 400 rpm for 60 minutes to promote coordination between the metal ions and the ligand, resulting in the formation of the bimetallic ZIF framework.

Following synthesis, the obtained powder was washed with methanol to remove unreacted precursors and residual ligand. The sample was dispersed in 30 mL of methanol, vortex-mixed at

2500 rpm for 3 minutes, and centrifuged at 3500 rpm for 15 minutes. This washing cycle was repeated three times. The collected precipitate was dried in an oven at 60 °C for approximately 16 hours, followed by vacuum drying at 120 °C for 16 hours to remove residual solvent and activate the porous structure.

3.3 Amine Functionalization Procedure

Amine functionalization of the synthesized ZIF materials was performed using ethylenediamine (EDA) through a post-synthetic impregnation method. This modification was carried out to introduce amine functional groups into the porous framework in order to enhance the interaction between the adsorbent surface and carbon dioxide molecules.

In a typical procedure, 1 g of the synthesized ZIF material was dispersed in 20 mL of methanol in a glass container. Ethylenediamine was then added to the solution to obtain the desired amine loading. Three different EDA loadings were prepared: 15 wt%, 30 wt%, and 45 wt%. For example, in the case of the 15 wt% sample, 0.15 g of ethylenediamine was added to the mixture containing 1 g of ZIF material.

The mixture was stirred using a magnetic stirrer for approximately 3 hours to allow the ethylenediamine molecules to diffuse into the pores of the ZIF structure and interact with the internal surfaces of the framework. This impregnation process allowed the amine molecules to be incorporated into the porous structure of the material.

After the functionalization process, the mixture was dried in an oven at 60 °C for 16 hours to remove excess methanol. The material was then further dried under vacuum at 120 °C for 16 hours to remove residual solvent and stabilize the amine-functionalized structure.

This functionalization procedure was applied to the high-entropy ZIF, ZIF-8, and bimetallic ZIF materials. The resulting amine-functionalized samples were subsequently used for structural characterization, surface area measurements, CO_2 adsorption analysis, and mixed-gas selectivity experiments.

3.4 Characterization Methods

The structural and textural properties of the synthesized ZIF materials were characterized using X-ray diffraction (XRD) and nitrogen adsorption-desorption analysis. These techniques were used to evaluate the crystallinity, surface area, and pore structure of the materials before and after amine functionalization.

3.5.1 X-ray Diffraction (XRD)

X-ray diffraction (XRD) analysis was conducted using a Proto Manufacturing AXRD Benchtop Powder X-ray Diffractometer to determine the crystalline structure and phase purity of the synthesized ZIF materials. The obtained diffraction patterns were used to confirm framework formation and assess the crystallinity of the samples. Powder XRD measurements were conducted using a diffractometer equipped with Cu Kα radiation. The diffraction patterns were recorded over a 2θ range of 5°-60°, which covers the characteristic diffraction peaks associated with ZIF structures. The obtained diffraction patterns were compared with reference patterns reported in the literature for ZIF-8 to verify successful framework formation. XRD analysis was carried out for all synthesized materials, including the pure ZIF samples (HE-ZIF, ZIF-8, and bimetallic ZIF) as well as the amine-functionalized samples containing 15 wt%, 30 wt%, and 45 wt% ethylenediamine (EDA). Comparison of the diffraction patterns allowed evaluation of the effects of mechanochemical synthesis conditions and amine loading on the crystallinity and structural

integrity of the ZIF materials. The XRD results were further used to determine the optimal synthesis conditions for HE-ZIF and to evaluate whether the framework structure was preserved after amine functionalization.

3.5.2 BET Surface Area and Porosity

The surface area and pore structure of the synthesized ZIF materials were analyzed using a Micromeritics TriStar II Surface Area and Porosity Analyzer through nitrogen adsorption-desorption measurements. This technique was used to evaluate the textural properties of the materials, including surface area, pore volume, and pore size distribution. Prior to measurement, the samples were degassed under vacuum at 120 °C for 16 hours to remove adsorbed moisture and residual solvent molecules from the pores. This activation step ensured that the internal pore structure of the materials was accessible for nitrogen adsorption. Nitrogen adsorption-desorption isotherms were obtained at liquid nitrogen temperature (77 K). The specific surface area of the samples was calculated using the Brunauer-Emmett-Teller (BET) method and reported in m^2/g. In addition, the total pore volume (cm^3/g) and maximum pore width (Å) were determined from the adsorption data to characterize the pore structure of the materials. BET measurements were conducted for all synthesized materials, including the pure ZIF samples (HE-ZIF, ZIF-8, and bimetallic ZIF) as well as their corresponding amine-functionalized samples containing 15 wt%, 30 wt%, and 45 wt% ethylenediamine (EDA). These measurements were used to evaluate the effect of amine functionalization on the surface area and pore structure of the ZIF materials. The BET analysis provided important information regarding the structural properties of the materials and helped explain variations in CO_2 adsorption performance observed during gas adsorption experiments.

3.6 CO_2 Adsorption Measurement

The CO_2 adsorption capacity of the synthesized ZIF materials was evaluated using a Micromeritics TriStar II Surface Area and Porosity Analyzer. The measurements were conducted to determine the amount of CO_2 adsorbed by each material at room temperature. Prior to measurement, the samples were degassed under vacuum at 120 °C for 16 hours to remove adsorbed moisture and residual solvent molecules from the pores. This activation step ensured that the internal surface area and pore structure of the materials were accessible for CO_2 adsorption. After degassing, CO_2 adsorption measurements were performed at room temperature, and the adsorption isotherm was obtained using the instrument. From the adsorption data, the total amount of CO_2 adsorbed by each sample was determined. The adsorption capacity was reported in mmol g^{-1}, representing the amount of CO_2 captured per gram of adsorbent. CO_2 adsorption experiments were carried out for all synthesized materials, including HE-ZIF, ZIF-8, and bimetallic ZIF, as well as their corresponding amine-functionalized samples containing 15 wt%, 30 wt%, and 45 wt% ethylenediamine (EDA). The adsorption results were used to compare the CO_2 capture performance of the different materials and to evaluate the influence of amine loading on adsorption capacity. The adsorption measurements provided important information regarding the CO_2 uptake behavior of the materials and were later used to analyze the relationship between surface area, pore structure, and gas adsorption performance.

3.7 CO_2 Selectivity Measurement

The preferential adsorption of CO_2 over other gases was evaluated through mixed-gas experiments coupled with mass spectrometry analysis using an MKS Cirrus 2 Mass Spectrometer. This approach enabled the assessment of CO_2 selectivity under competitive adsorption conditions in a multi-component gas system. A mixed gas stream consisting of CO_2, CH_4, and He was used

for the selectivity experiment. Each gas was introduced at a flow rate of 20 mL/min using mass flow controllers, resulting in a total flow rate of 60 mL/min and an initial gas composition of approximately 33.33% CO_2, 33.33% CH_4, and 33.33% He. For the adsorption experiment, 0.4 g of the adsorbent material was packed into a glass tube (internal diameter ~0.35 inches, length 30 inches) and secured in place using glass wool. The packed tube was then placed inside a tube furnace, allowing precise control of the system temperature during the experiment. The mixed gas stream was first analyzed using the mass spectrometer in bypass mode for 5 minutes to establish the baseline gas composition. The gas mixture was then passed through the packed adsorption tube containing the ZIF material for 60 minutes, during which the outlet gas composition was continuously monitored using the mass spectrometer. Finally, the system was returned to bypass mode for an additional 5 minutes to confirm the outlet composition after adsorption. The selectivity behavior of the material was determined by comparing the outlet gas composition with the baseline mixture. A decrease in CO_2 concentration at the outlet relative to CH_4 and He indicated preferential adsorption of CO_2 by the adsorbent. The adsorption experiments were conducted at two different temperatures, 20 °C and 100 °C, to evaluate the influence of temperature on CO_2 selectivity. Each adsorption test was carried out for approximately one hour to ensure that the adsorption behavior reached a stable condition. These selectivity measurements were performed for all synthesized materials, including HE-ZIF, ZIF-8, and bimetallic ZIF, as well as their corresponding amine-functionalized samples containing 15 wt%, 30 wt%, and 45 wt% ethylenediamine (EDA). The results were used to compare the CO_2 selectivity of the different materials and to evaluate the effect of amine functionalization and temperature on gas separation performance.

3.9 Regeneration and Cyclic Stability Test

The regeneration ability and cyclic stability of the synthesized adsorbents were evaluated through repeated CO_2 adsorption-desorption cycles. The experiment was conducted to determine whether the materials could maintain their adsorption performance after multiple regeneration steps. For this purpose, HE-ZIF, bimetallic ZIF, and ZIF-8 samples were subjected to seven consecutive adsorption-desorption cycles. In each cycle, CO_2 adsorption measurements were first performed using the Micromeritics Surface Area and Porosity Analyzer at room temperature to determine the CO_2 adsorption capacity of the sample. After completion of the adsorption measurement, the CO_2-loaded sample was removed from the instrument and regenerated to remove the adsorbed CO_2 molecules. Regeneration was carried out in a vacuum oven at 170 °C for 16 hours, which allowed desorption of the adsorbed gas and reactivation of the porous structure. Following regeneration, the sample was cooled to room temperature under a nitrogen (N_2) atmosphere and subjected to the next CO_2 adsorption cycle under the same experimental conditions. This procedure was repeated for a total of seven adsorption-desorption cycles. The adsorption capacity obtained in each cycle was compared to evaluate the stability and reusability of the materials. The regeneration study provided insight into the durability of the synthesized ZIF materials and their potential applicability for repeated CO_2 capture operations.

Chapter 4 - Results and Discussion

4.1 Optimization of HE-ZIF Synthesis

To determine the optimal synthesis conditions for HE-ZIF, the effect of milling time on the crystallinity and CO_2 adsorption performance of the material was investigated. HE-ZIF samples prepared at different milling times (HZ-40, HZ-60, and HZ-90) were compared with a reference ZIF-8 sample (Z8-60).

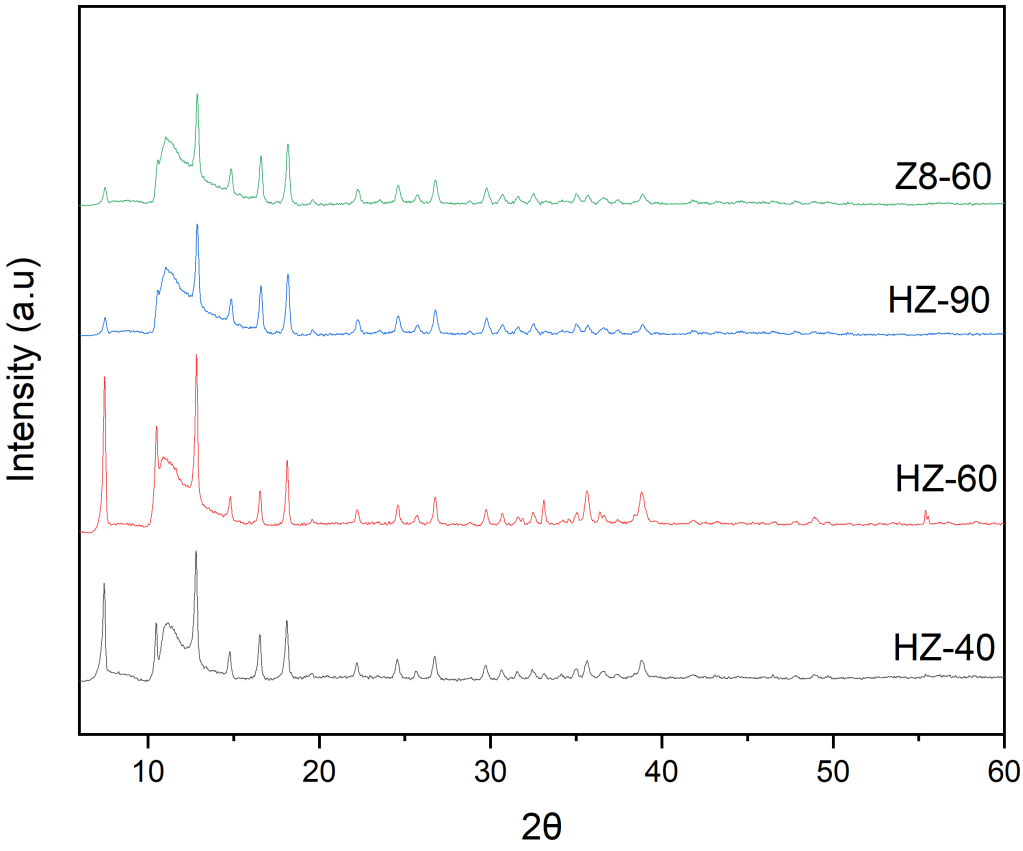

Figure 4.1 XRD patterns of ZIF samples synthesized at three different milling times.

The structural properties of these samples were analyzed using X-ray diffraction (XRD), and the patterns are shown in Figure 4.1. All samples exhibit diffraction peaks consistent with the

characteristic crystal structure of Z8-60, indicating that the mechanochemical synthesis successfully produced ZIF-type frameworks despite the presence of multiple metal species. The major peaks appear at approximately 7.3°, 10.4°, 12.6°, 16.5°, and 18.0°, corresponding to the (011), (002), (112), (013), and (222) crystallographic planes associated with the sodalite (SOD) topology typical of ZIF-8 materials. However, differences in peak intensity and sharpness were observed among the samples. The HZ-60 sample exhibited the highest peak intensity and sharpest peaks, indicating a higher degree of crystallinity. In comparison, HZ-40 showed broader and weaker peaks, suggesting incomplete framework formation due to insufficient milling time, while HZ-90 displayed slightly reduced peak intensity, which may result from structural disorder caused by excessive mechanical energy during prolonged milling. To further investigate the effect of milling time on adsorption behavior, CO_2 adsorption measurements were performed, and the results are presented in Figure 4.2.

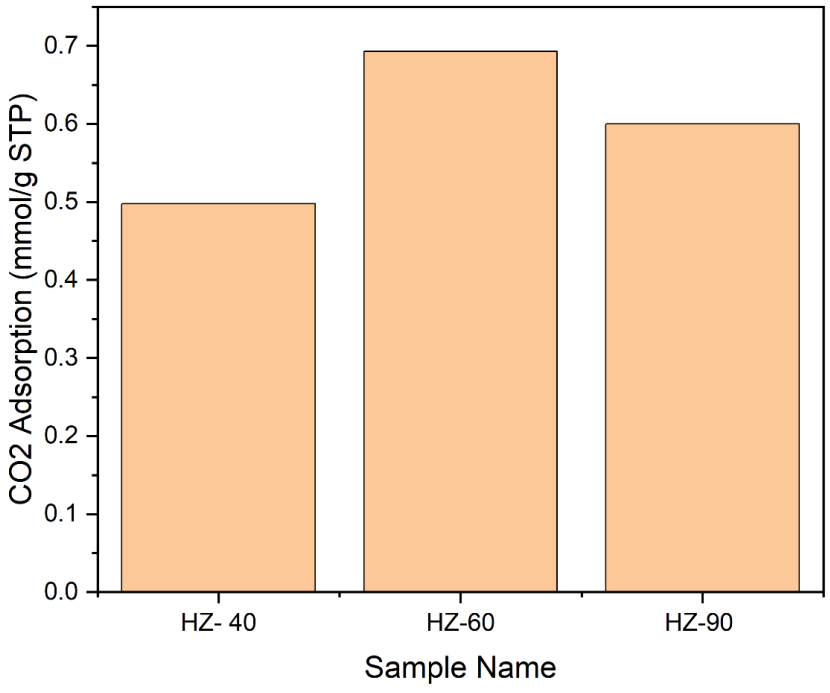

Figure 4.2 XRD patterns of ZIF samples synthesized at three different milling times.

The measured CO_2 adsorption capacities were 0.4976 mmol g^{-1} for HZ-40, 0.6929 mmol g^{-1} for HZ-60, and 0.6081 mmol g^{-1} for HZ-90. Among the three samples, HZ-60 exhibited the highest CO_2 adsorption capacity, which is consistent with its superior crystallinity observed in the XRD analysis. Crystallinity mainly controls how well-defined and accessible the designed pore system is. The lower adsorption capacity of HZ-40 is likely due to incomplete framework formation, resulting in reduced pore accessibility. under-milling leaves partially reacted or poorly crystalline material with low porosity, so CO_2 uptake is lower. This type of behavior is seen in several mechanochemical MOF systems where the best CO_2 capacity coincides with the condition giving highest crystallinity and ultramicropore volume [142–144]. In contrast, the slightly lower adsorption of HZ-90 compared to HZ-60 may be attributed to structural deformation, reduced micropore volume and phase transformation caused by over-milling [145–147]. These results indicate that an optimal milling duration is required to achieve a balance between complete framework formation and structural stability. Based on both XRD analysis and CO_2 adsorption performance, the HZ-60 sample was selected as the optimized HE-ZIF material for subsequent amine functionalization and further adsorption studies.

4.2 Structural Characterization of ZIF Materials

The crystal structures of the synthesized ZIF materials were analyzed using X-ray diffraction (XRD) to evaluate the formation of the framework and the effect of metal composition and amine functionalization on structural stability. The XRD patterns of ZIF-8 (Z8-60), high-entropy ZIF (HZ-60), and bimetallic ZIF (BZ-60) synthesized using a 60-minute milling time are shown in Figure 4.3, while the XRD patterns of the amine-functionalized samples are presented in

Figures 4.4, 4.5, and 4.6 for ZIF-8, bimetallic ZIF, and HE-ZIF, respectively.

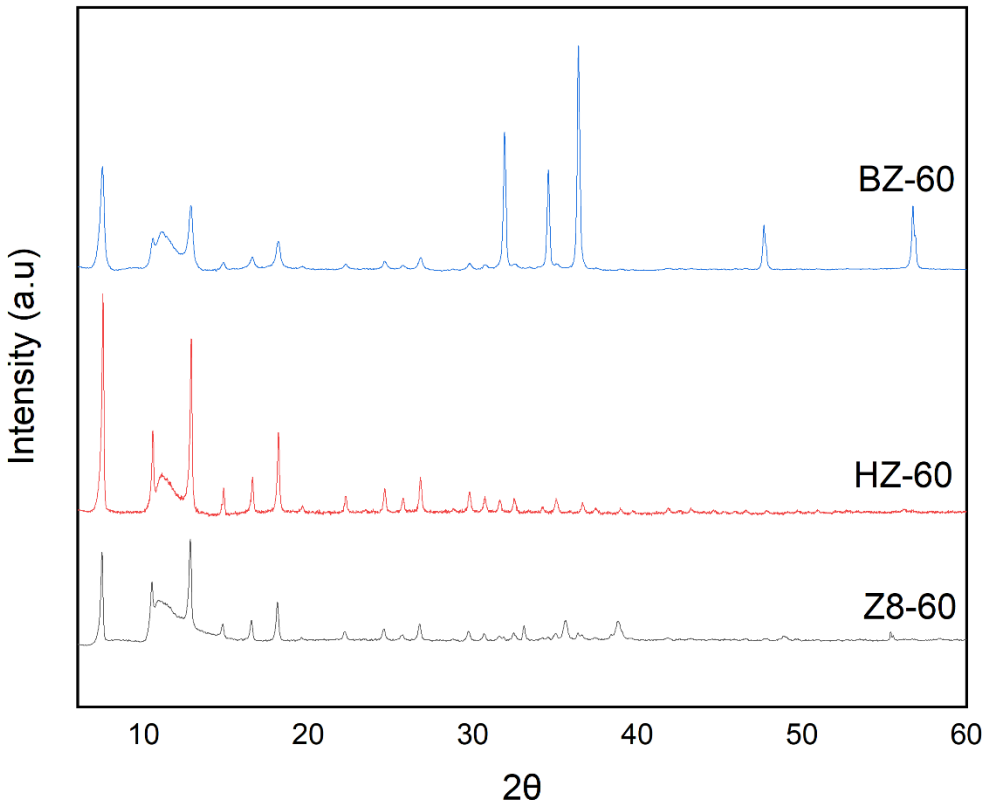

Figure 4.3 XRD patterns of ZIF-8 (Z8-60), HE-ZIF (HZ-60), and bimetallic ZIF (BZ-60)

As shown in Figure 4.3, all synthesized samples exhibit diffraction peaks consistent with the characteristic ZIF-8 crystal structure, confirming successful formation of the framework through mechanochemical synthesis. The major peaks appear at approximately 7.3°, 10.4°, 12.6°, 16.5°, and 18.0°, corresponding to the (011), (002), (112), (013), and (222) crystallographic planes associated with the sodalite (SOD) topology. The presence of these peaks in Z8-60, BZ-60, and HZ-60 indicates that the incorporation of multiple metal ions in the bimetallic and high-entropy systems does not disrupt the fundamental ZIF framework. Although the overall structure remains similar, slight variations in peak intensity are observed among the samples, which may arise from differences in metal composition and crystallinity.

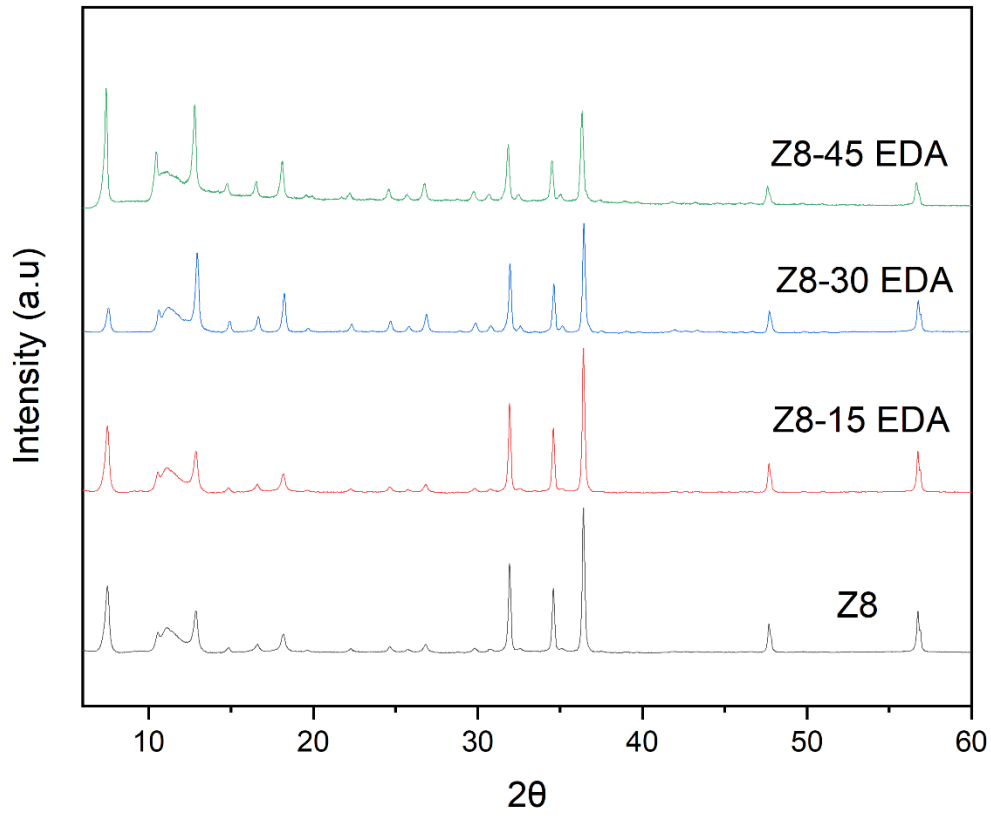

Figure 4.4 XRD patterns of ZIF-8 before and after ethylenediamine (EDA) functionalization at 15, 30, and 45 wt% loadings.

As shown in Figure 4.4, the XRD patterns of ZIF-8 after EDA functionalization (Z8-15EDA, Z8-30EDA, and Z8-45EDA) retain the characteristic diffraction peaks of the ZIF-8 SOD topology, indicating that the framework structure remains intact after amine loading. However, a gradual decrease in peak intensity is observed with increasing EDA content, with crystallinity beginning to decline from Z8-30EDA. This behavior is attributed to the incorporation of amine molecules within the pores, leading to partial pore filling and increased structural disorder [148]. Additionally, excess amine groups can compete with 2-methylimidazole for Zn(II), altering local coordination and generating defects or mixed phases [149,150]. At higher amine loadings, the formation of Zn-amine or Zn-acetate species and framework distortion further disrupts crystallinity

[149]. These structural changes reduce coherent scattering, resulting in broader and less intense XRD peaks while the overall topology remains preserved.

A

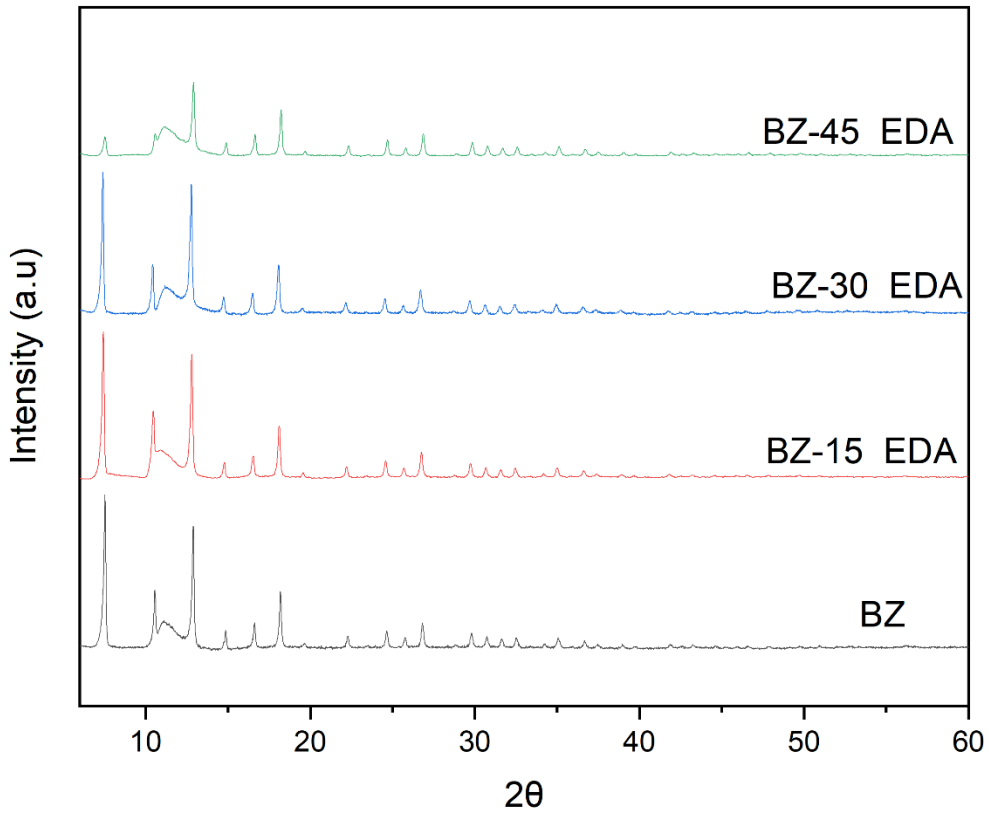

Figure 4.5 XRD patterns of BZ before and after ethylenediamine (EDA) functionalization at 15, 30, and 45 wt% loadings.

similar trend is observed for the BZ samples shown in Figure 4.5. The diffraction peaks of BZ-15EDA, BZ-30EDA, and BZ-45EDA remain consistent with those of the parent BZ, indicating that EDA functionalization preserves the overall crystal structure. However, a gradual decrease in peak intensity is evident with increasing amine loading, suggesting reduced crystallinity due to pore filling, increased structural disorder, and partial occupation of active sites. Additionally, competitive coordination of amine groups with 2-methylimidazole at Zn(II) centers, along with the possible formation of secondary Zn–amine or Zn–acetate phases, further disrupts the framework and contributes to peak broadening and intensity loss. This effect is more pronounced at higher loadings (45 wt% EDA), where the incorporation of EDA within the micropores and on

the internal surface likely introduces structural disorder and partially occupies pore space, leading to diminished diffraction intensity.

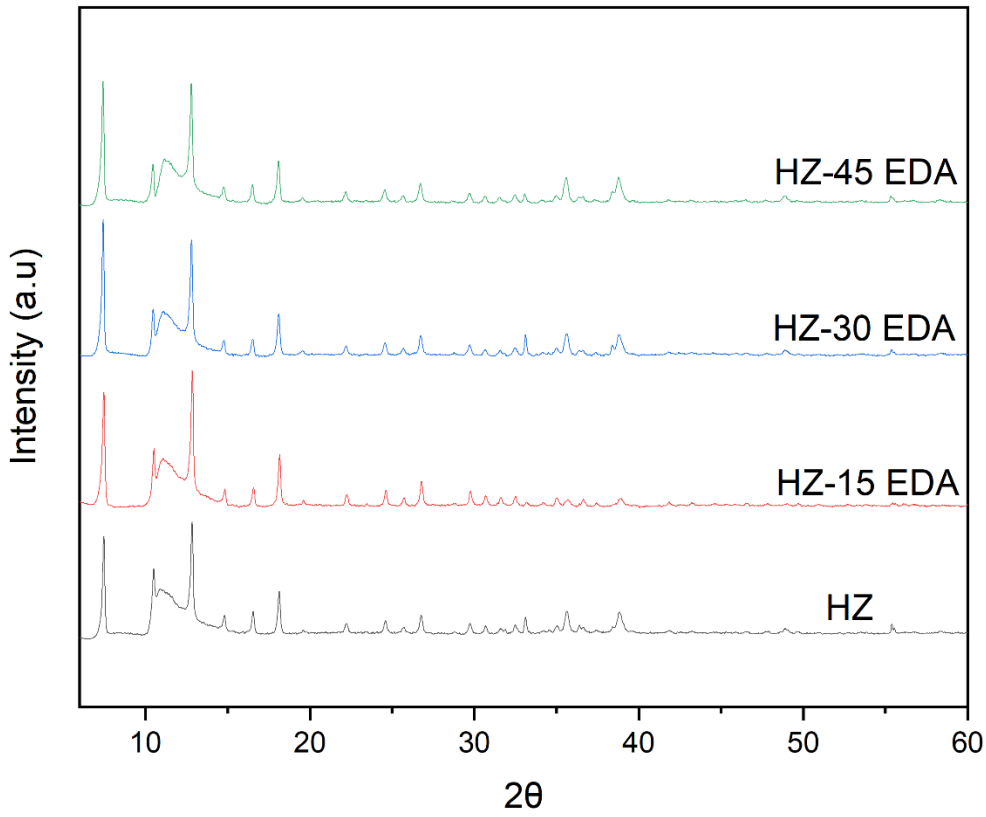

Figure 4.6 XRD patterns of HZ before and after ethylenediamine (EDA) functionalization at 15, 30, and 45 wt% loadings.

The XRD patterns of HE-ZIF (HZ) and its amine-functionalized samples (HZ-15EDA, HZ-30EDA, and HZ-45EDA) are shown in Figure 4.6. The major diffraction peaks remain consistent across all samples, indicating that the fundamental crystal structure of HZ is preserved after EDA functionalization. At low amine loading (HZ-15EDA), the peaks remain sharp with slightly increased intensity, suggesting improved ordering or surface interaction without structural disruption. This may be attributed to partial pore reopening and enhanced accessibility at low amine content, which can improve apparent crystallinity [148].

However, with increasing EDA loading (HZ-30EDA and HZ-45EDA), a noticeable reduction in peak intensity and slight broadening are observed, indicating a gradual decline in crystallinity. This behavior can be attributed to the incorporation of EDA molecules within the micropores and on the internal surface, which introduces structural disorder and partially occupies pore space. The effect is more pronounced at higher loadings, where excessive amine content leads to pore blocking, framework distortion, and a reduction in overall crystallinity.

4.3 Porosity and Surface Area Analysis

The porosity characteristics of the synthesized ZIF materials were evaluated using N_2 adsorption-desorption measurements obtained from a Micromeritics surface area and porosity analyzer.

Table 4. 1 Surface area, total pore volume, and maximum pore width of synthesized ZIF materials.

Sample Name	Surface Area (m^2/g)	Total Pore Volume (cm^3/g)	Maximum Pore width (Å)
Z8	804.0344	0.429	376.546
Z8-15EDA	840.410	0.431	366.173
BZ	1154.727	0.587	388.895
HZ	1063.146	0.572	366.058
HZ-15EDA	1187.108	0.620	372.579
HZ-30 EDA	848.288	0.455	367.235
HZ-45 EDA	745.567	0.405	358.793

As shown in Table 4.1, the parent ZIF materials exhibit relatively high BET surface areas typical of microporous ZIF frameworks. Among the three materials, bimetallic ZIF (BZ) shows the highest surface area (1154.7 m^2g^{-1}), followed by HE-ZIF (HZ) with 1063.1 m^2g^{-1}, while ZIF-8 (Z8) exhibits a comparatively lower surface area (806.6 m^2g^{-1}). The bimetallic ZIF also shows the largest total pore volume (0.5868 cm^3 g^{-1}) and maximum pore width (388.9 Å), indicating a more accessible pore structure. The higher surface area and porosity of BZ compared to ZIF-8 can be attributed to metal mixing (Zn^{2+}/Co^{2+}), which modifies nucleation and crystal growth behavior while preserving the SOD topology [151,152]. This often leads to smaller and more uniform crystals, increased interparticle voids, and the development of hierarchical micro-mesoporous structures, thereby enhancing accessible surface area and pore volume [153,154]. In the case of HE-ZIF, the incorporation of multiple metal species introduces greater structural disorder and defect sites. While the framework still retains the open SOD topology and remains highly microporous, resulting in a higher surface area than ZIF-8, excessive disorder and partial pore blocking can limit pore accessibility compared to the more optimally organized bimetallic system [155–157]. As a result, HZ exhibits an intermediate surface area between ZIF-8 and BZ.

These results suggest that the incorporation of additional metal centers can influence the development of the porous framework and increase the accessible surface area.

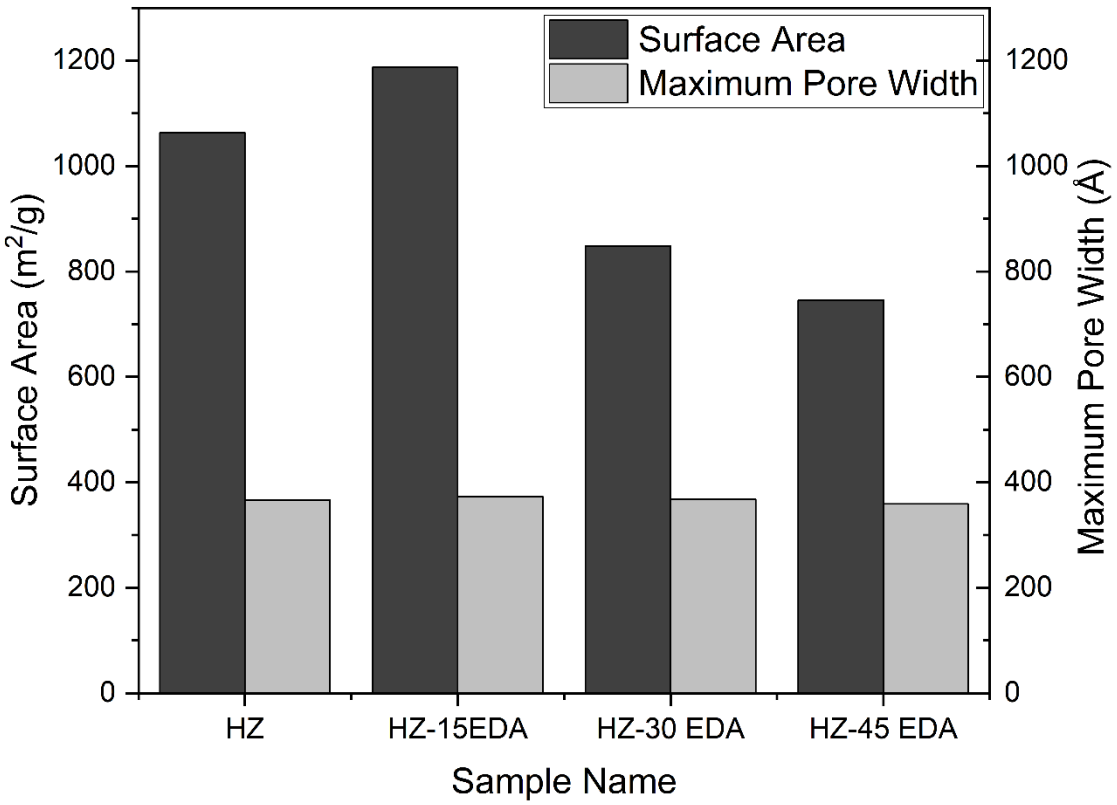

Figure 4.7 Effect of EDA loading on BET surface area and maximum pore width of HE-ZIF samples.

The influence of amine functionalization on the HE-ZIF structure is presented in Figure 4.7. The introduction of 15 wt% EDA (HZ-15EDA) slightly increases the BET surface area to 1187.1 $m^2 g^{-1}$. This enhancement can be attributed to the removal of occluded species or reopening of previously inaccessible micropores, along with slight changes in particle packing that create additional interparticle voids [148]. However, increasing the EDA loading to 30 wt% and 45 wt% results in a noticeable reduction in surface area, as shown in Table 4.1 and Figure 4.7. This decrease is due to partial pore occupation and blocking by amine molecules, as well as narrowing of pore windows through coordinated or tethered amines, which limits accessibility to the microporous network [148,158]. At higher loadings, excessive amine incorporation can also

introduce structural defects and reduce crystallinity, further decreasing the effective pore volume and surface area . Overall, the results indicate that amine functionalization strongly influences the porosity of HE-ZIF, with an optimal loading level where pore accessibility is preserved while functional groups are successfully introduced.

4.4 CO_2 Adsorption Performance and Effect of Amine Loading

The CO_2 adsorption performance of the synthesized ZIF materials was evaluated to understand the influence of framework composition and amine functionalization.

Table 4.2 CO_2 adsorption capacities of Z8, BZ, and HZ before and after EDA functionalization (0-45 wt%) at STP

Material	Samples	CO_2 Adsorption (mmol g^{-1} STP)
ZIF-8	Z8	0.413
	Z8-15EDA	0.533
	Z8-30EDA	0.639
	Z8-45EDA	0.550
Bimetallic ZIF	BZ	0.791
	BZ-15EDA	0.802
	BZ-30EDA	0.788
	BZ-45EDA	0.808
HE-ZIF	HZ	0.693
	HZ-15EDA	0.811

	HZ-30EDA	0.537
	HZ-45EDA	0.479

As shown in Table 4.2, the parent materials exhibit distinct CO_2 adsorption behaviors. Among the unmodified samples, bimetallic ZIF (BZ) shows the highest CO_2 uptake (0.7912 mmol g^{-1}), followed by HE-ZIF (HZ, 0.6929 mmol g^{-1}), while ZIF-8 (Z8) exhibits the lowest adsorption (0.4127 mmol g^{-1}). This trend is consistent with the porosity results discussed in Section 4.3, where higher surface area and pore volume provide more accessible adsorption sites. In these parent materials, CO_2 uptake is primarily governed by physisorption, driven by van der Waals interactions within the microporous structure. Upon EDA functionalization, the adsorption capacities change significantly, as summarized in Table 4.2. For ZIF-8, CO_2 uptake increases from 0.4127 mmol g^{-1} (Z8) to 0.6384 mmol g^{-1} (Z8-30EDA), followed by a slight decrease at higher loading (0.5500 mmol g^{-1} for Z8-45EDA). In contrast, bimetallic ZIF shows relatively stable adsorption values (0.7879-0.8081mmol g^{-1}) across different EDA loadings. For HE-ZIF, adsorption initially increases from 0.6929 mmol g^{-1} (HZ) to 0.8108 mmol g^{-1} (HZ-15EDA), but then decreases significantly at higher loadings (0.5373 mmol g^{-1} for HZ-30EDA and 0.4787 mmol g^{-1} for HZ-45EDA).

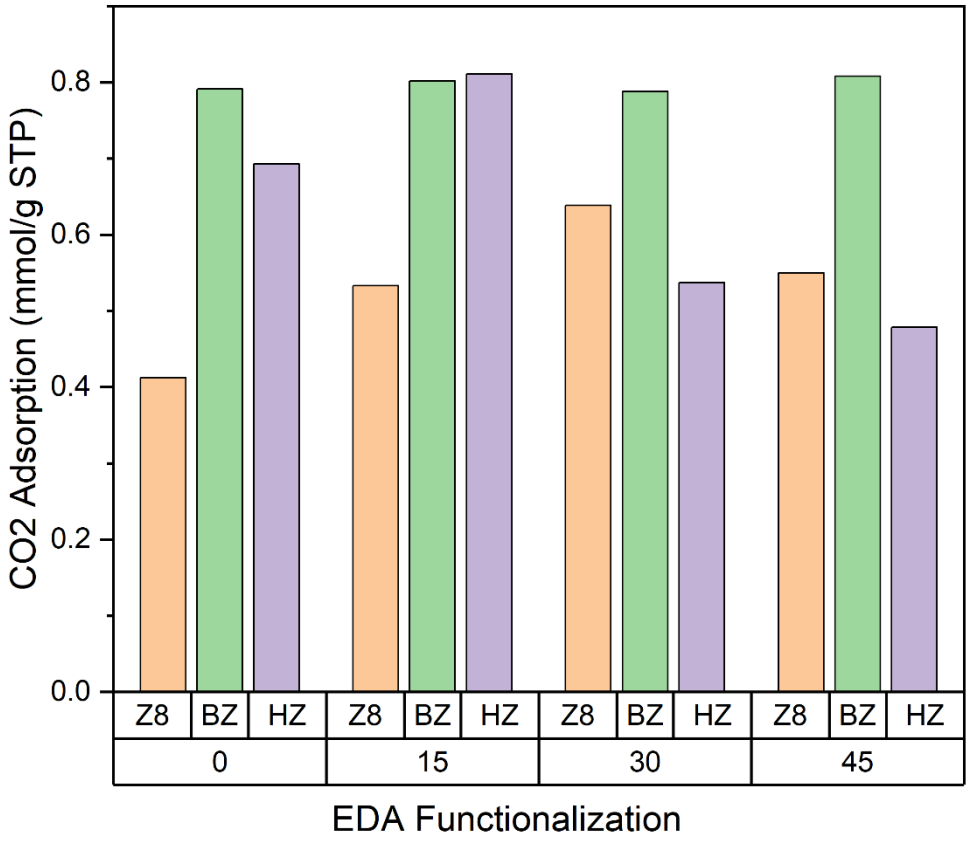

Figure 4.8 CO2 adsorption of Z8, BZ, and HZ as a function of EDA loading (0–45 wt%)

These variations are more clearly visualized in Figure 4.8, which illustrates the trend of CO_2 adsorption as a function of EDA loading. The figures show that ZIF-8 experiences a moderate increase in adsorption with increasing amine content up to an optimal loading, after which a decline occurs. Bimetallic ZIF exhibits minimal variation, maintaining consistently high adsorption across all loadings. In contrast, HE-ZIF demonstrates a pronounced peak at low EDA loading (15 wt%), followed by a sharp decrease at higher loadings.

The observed trends arise from the balance between physisorption and chemisorption. The introduction of ethylenediamine (EDA) provides amine functional groups ($–NH_2$), which create additional high-affinity adsorption sites through acid–base interactions, hydrogen bonding, and

reversible carbamate or bicarbonate formation. At low to moderate loadings, these interactions increase the binding strength and enhance CO_2 uptake, sometimes aided by slight pore reopening or improved accessibility. However, as amine loading increases, the molecules progressively occupy and obstruct micropores, reducing available pore volume and limiting CO_2 diffusion into the framework. In addition, each amine group can bind only a limited amount of CO_2, so excess amine does not proportionally increase capacity but instead displaces free adsorption space.

This effect is particularly pronounced in HE-ZIF, where the more defect-rich and sensitive pore structure is more easily disrupted by amine incorporation, leading to a sharp decline in adsorption at higher loadings. In contrast, bimetallic ZIF maintains relatively stable performance due to its higher and more robust porosity, which better accommodates amine groups without significant loss of accessible adsorption sites.

4.5 CO_2 Selectivity Analysis at Ambient Temperature

The CO_2 selectivity of ZIF-8 (Z8), bimetallic ZIF (BZ), and high-entropy ZIF (HZ) materials were evaluated at ambient temperature (20 °C) using mass spectrometry (MS) by monitoring the inlet and outlet gas compositions. The selectivity is expressed as CO_2 removal (%), calculated from the reduction in CO_2 concentration between the feed and outlet streams.

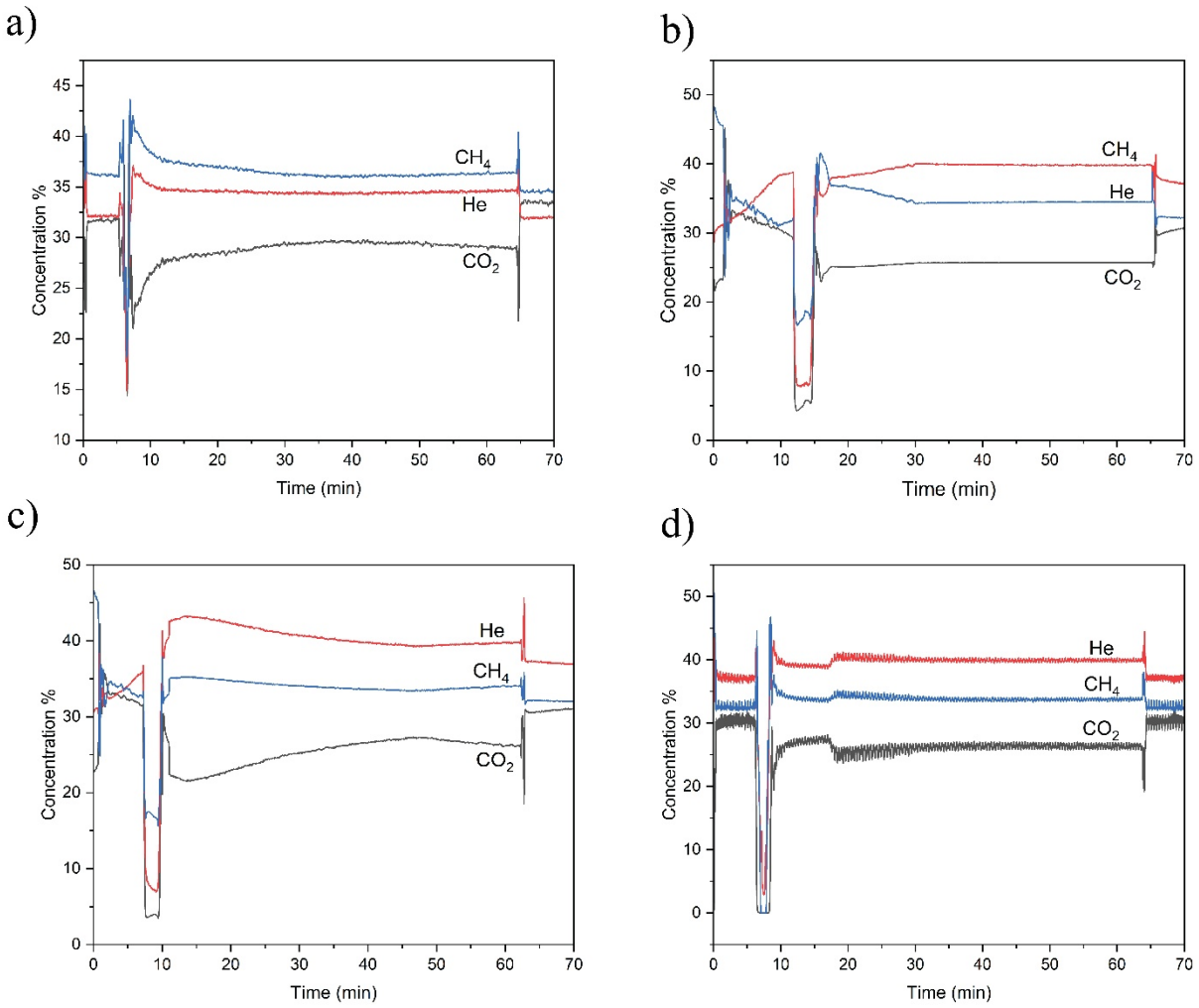

Figure 4.9 Mass spectrometry profiles of CO2, CH4, and He gas concentrations for (a) Z8, (b) Z8-15EDA, (c) Z8-30EDA, and (d) Z8-45EDA at 20 °C

The dynamic breakthrough profiles for the Z8 series are shown in Figure 4.9. A relatively small decrease in CO_2 concentration is observed after introducing the adsorption bed, indicating limited adsorption capacity. For example, in Figure 4.9(c) (Z8-30EDA), the CO_2 concentration decreased from 30.933% at the inlet to 25.324% at the outlet. In contrast, CH_4 and He concentrations remained nearly unchanged, demonstrating negligible adsorption of these gases and confirming selective CO_2 uptake. However, the overall selectivity remains low due to the limited interaction strength between CO_2 and the ZIF-8 framework.

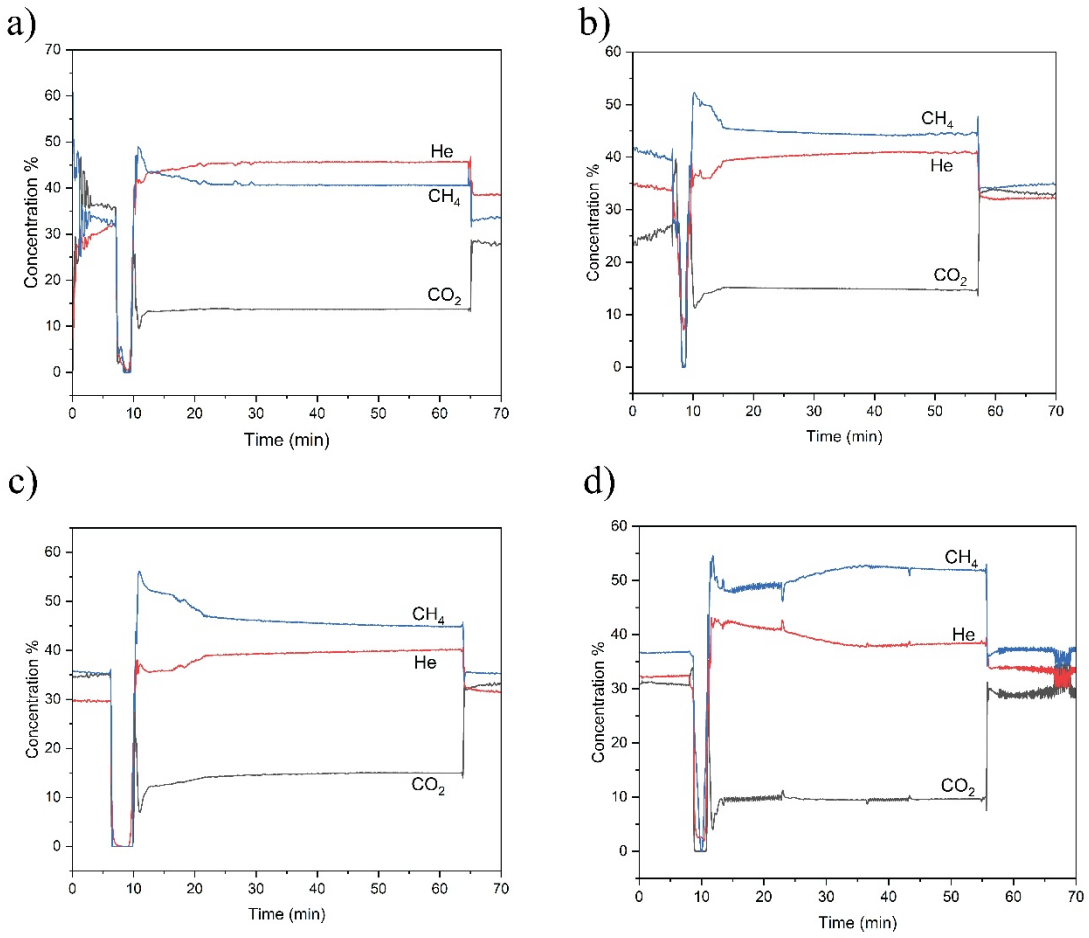

Figure 4.10 Mass spectrometry profiles of outlet CO2, CH4, and He concentrations for (a) BZ, (b) BZ-15EDA, (c) BZ-30EDA, and (d) BZ-45EDA at 20 °C

In contrast, the BZ series in Figure 4.10 exhibits significantly enhanced CO_2 adsorption. A pronounced drop in CO_2 concentration is observed upon passing through the adsorbent bed, while CH_4 and He show minimal variation. Notably, in Figure 4.10(d) (BZ-45EDA), the CO_2 concentration decreases sharply from 29.718% to 9.637%, indicating strong CO_2 capture. This improvement is attributed to the combined effect of the bimetallic framework and amine functionalization, which increases the number of active adsorption sites while maintaining sufficient pore accessibility.

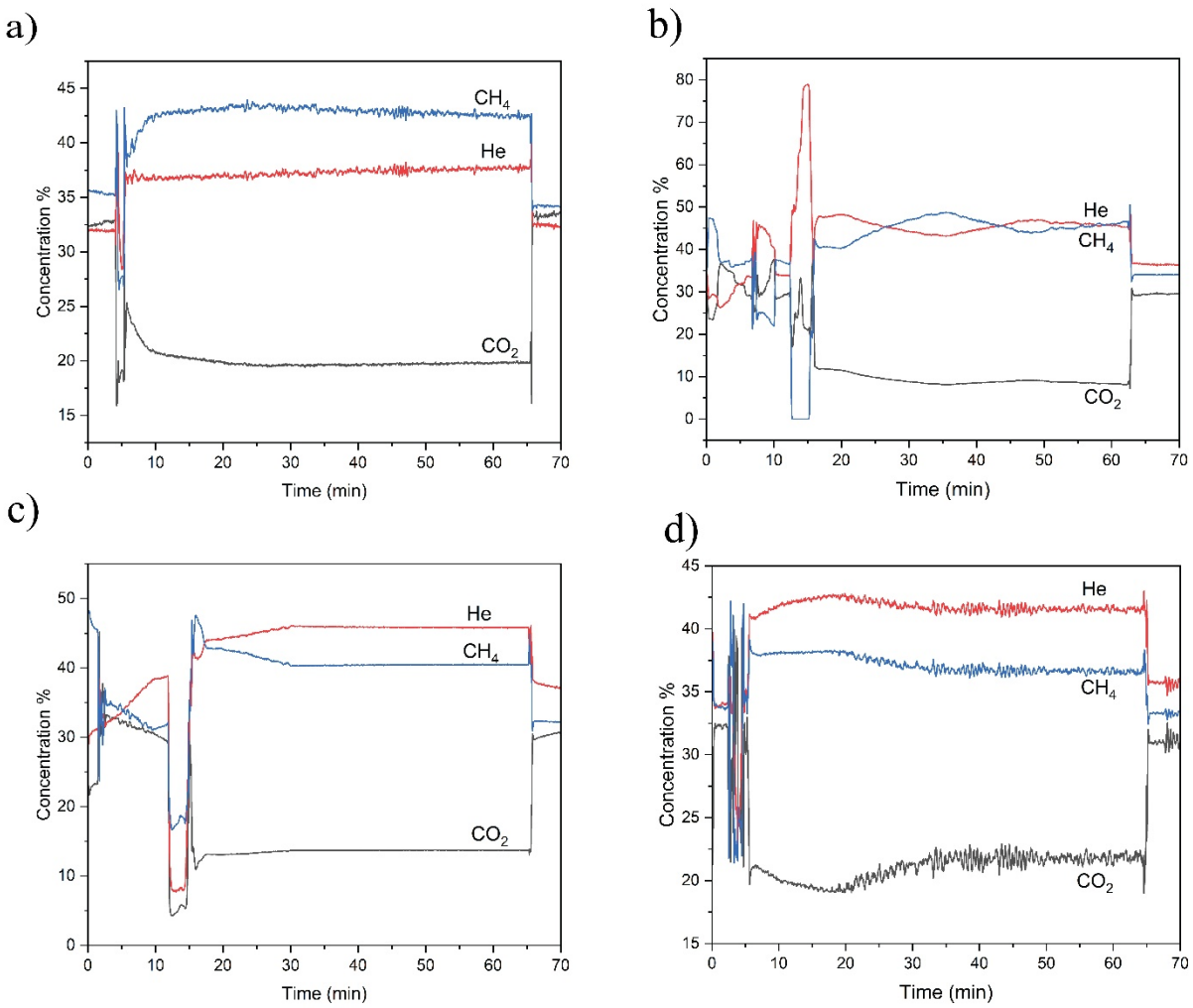

Figure 4.11 Mass spectrometry profiles of outlet CO2, CH4, and He concentrations for (a) HZ, (b) HZ-15EDA, (c) HZ-30EDA, and (d) HZ-45EDA at 20 °C

Similarly, the HZ series presented in Figure 4.11 demonstrates strong CO_2 adsorption at moderate amine loading. In Figure 4.11(b) (HZ-15EDA), the CO_2 concentration drops from 29.477% at the inlet to 9.156% at the outlet, representing one of the highest adsorption performances among all samples. However, at higher amine loading, the reduction in CO_2 concentration becomes less significant, suggesting that excessive amine content leads to pore blockage and restricts gas diffusion.

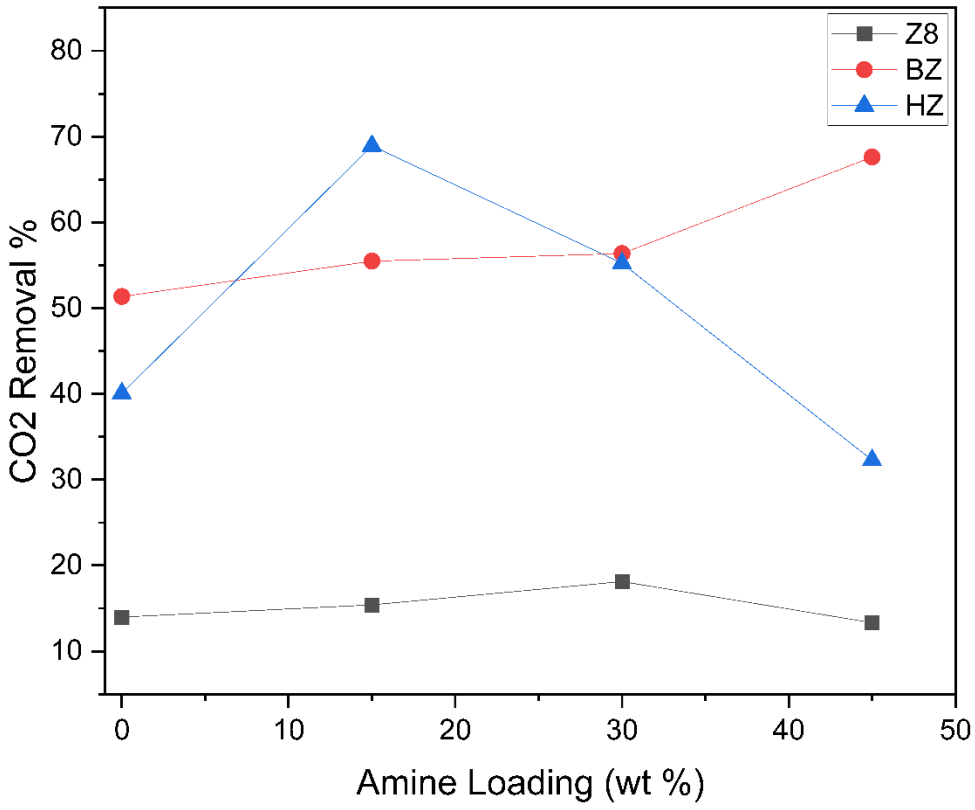

Figure 4.12 CO_2 removal (%) of Z8, BZ, and HZ as a function of amine loading (wt%) at 20 °C

A quantitative comparison of CO_2 removal as a function of amine loading is summarized in Figure 4.12. The Z8 samples exhibit low CO_2 removal (13–18%), with only slight improvement at moderate loading. In contrast, BZ shows consistently high CO_2 removal, increasing from ~51% to ~68% with increasing amine content, with BZ-45EDA achieving the highest performance. The HZ samples display optimal behavior at 15 wt% EDA (~69%), after which the removal decreases significantly at higher loadings.

The superior selective CO_2 adsorption observed in BZ-45EDA and HZ-15EDA compared to CH_4 and He arises from the combined effects of framework structure and amine functionality. CO_2 possesses a significant quadrupole moment, enabling stronger interactions with polar surfaces and amine groups, whereas CH_4 is nonpolar and He is inert, interacting only through weak

dispersion forces. The introduction of EDA provides primary amine groups that enhance CO_2 affinity through acid–base interactions, hydrogen bonding, and possible carbamate formation, thereby increasing the isosteric heat of adsorption and creating CO_2 specific binding sites. Since CH_4 and He are not significantly affected by these functional groups, CO_2 adsorption increases more selectively, improving CO_2/CH_4 and CO_2/He separation performance.

In BZ-45EDA, the bimetallic framework maintains higher pore accessibility and structural robustness even at elevated amine loading, allowing efficient diffusion while accommodating a large number of active amine sites. In HZ-15EDA, an optimal balance between preserved microporosity and introduced amine functionality is achieved, where additional CO_2 specific sites enhance adsorption without significantly restricting pore accessibility.

At higher amine loadings, however, excessive EDA begins to occupy and narrow the pore network, reducing micropore volume and limiting gas diffusion. Crowding of amine chains can make some adsorption sites sterically inaccessible and reduce overall pore accessibility, leading to a decline in CO_2 uptake and separation performance despite the higher amine content. As a result, CO_2 removal and selectivity pass through an optimum at moderate loading and decrease at higher amine concentrations, particularly in the more structurally sensitive HE-ZIF system.

4.6 CO_2 Selectivity at Elevated Temperature

The effect of temperature on CO_2 selectivity was investigated at 100 °C using mass spectrometry (MS) and compared with the results obtained at ambient temperature (20 °C). The dynamic breakthrough profiles for selected samples are shown in Figures 4.13 and 4.14, while the corresponding CO_2 removal efficiencies are summarized in Figure 4.15.

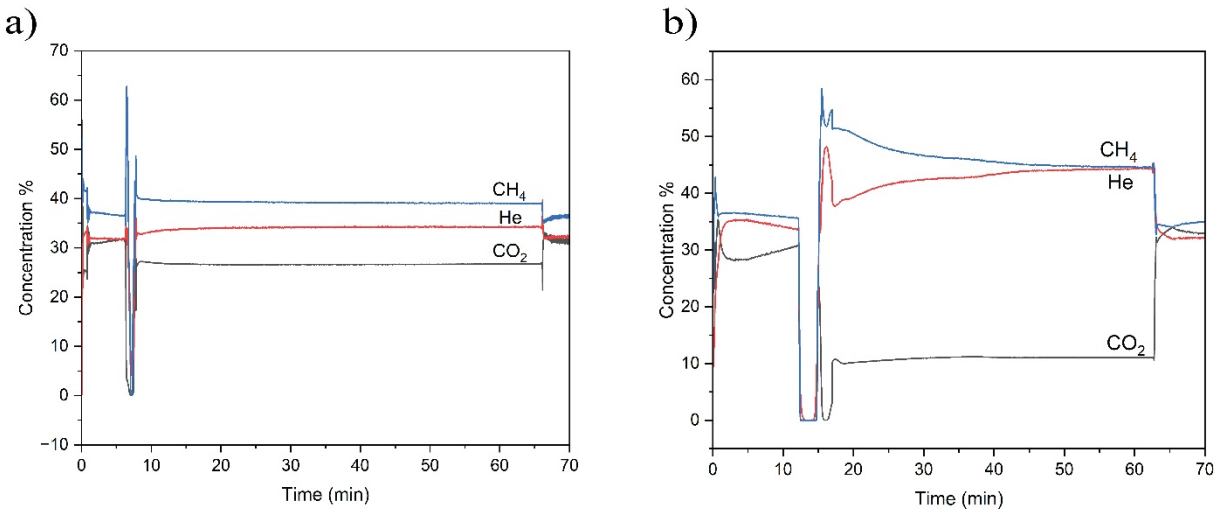

Figure 4.13 Mass spectrometry profiles of outlet CO_2, CH_4, and He concentrations for (a) Z8-30EDA and (b) BZ-45EDA at 100 °C.

As shown in Figure 4.13(a), the Z8-30EDA sample exhibits a relatively small decrease in CO_2 concentration, from 31.671% at the inlet to 26.676% at the outlet, indicating weak adsorption performance at elevated temperature. In contrast, Figure 4.13(b) shows that BZ-45EDA demonstrates a much stronger reduction in CO_2 concentration, decreasing from 34.326% to 14.044%, confirming its superior adsorption capability even at 100 °C.

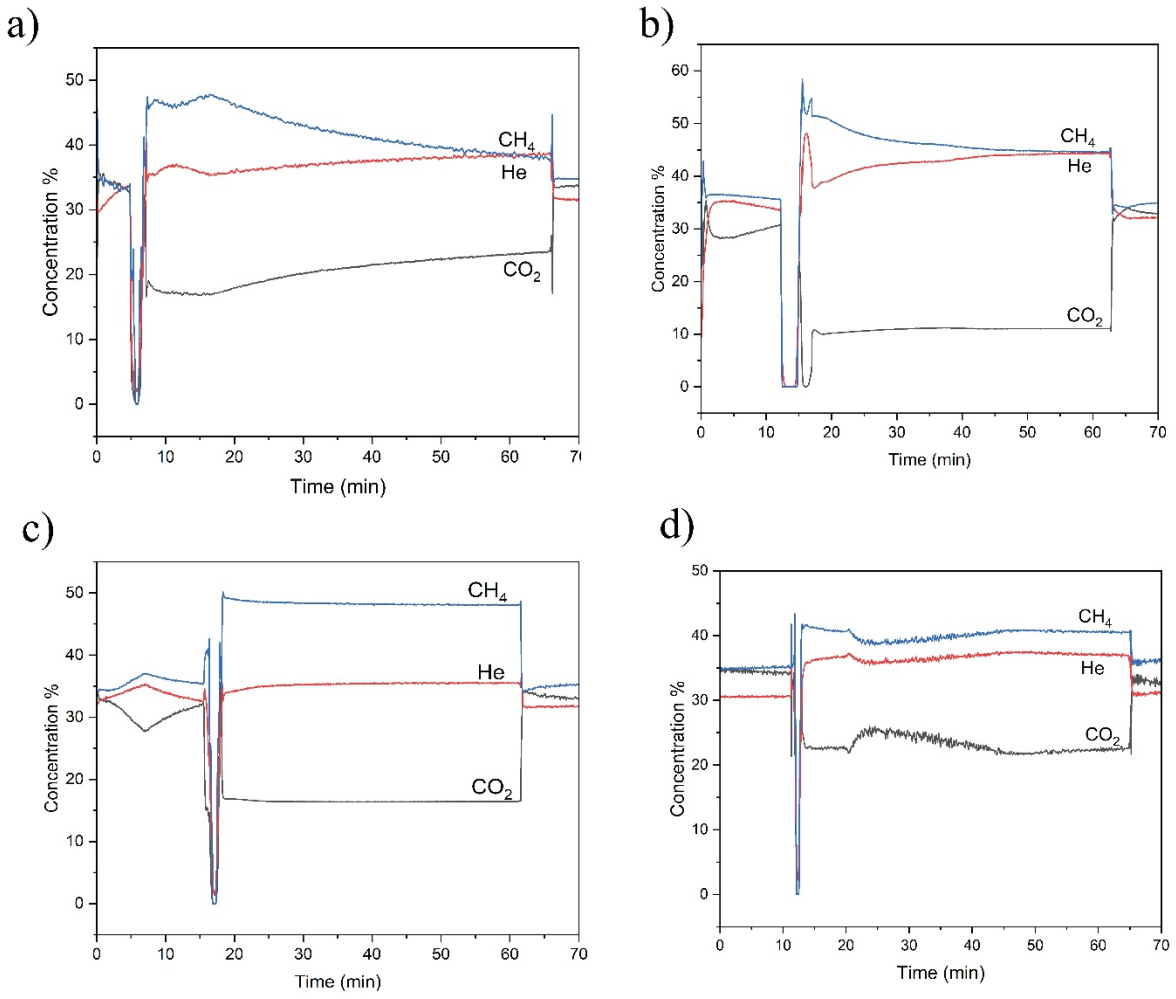

Figure 4.14 Mass spectrometry profiles of outlet CO_2, CH_4, and He concentrations for (a) HZ, (b) HZ-15EDA, (c) HZ-30EDA, (d) HZ-45EDA,

The behavior of HE-ZIF materials is presented in Figure 4.14. The parent HZ sample (Figure 4.14a) shows negligible CO_2 adsorption, with the outlet concentration (38.825%) exceeding the inlet concentration (33.603%), indicating minimal uptake and possible displacement

of pre-adsorbed gases. However, significant improvement is observed upon amine functionalization. For HZ-15EDA (Figure 4.14b), the CO_2 concentration decreases sharply from 33.127% to 10.905%, demonstrating excellent adsorption performance. Similarly, HZ-30EDA (Figure 4.14c) shows a reduction from 33.304% to 16.462%, while HZ-45EDA (Figure 4.14d) exhibits a decrease from 32.949% to 23.088%.

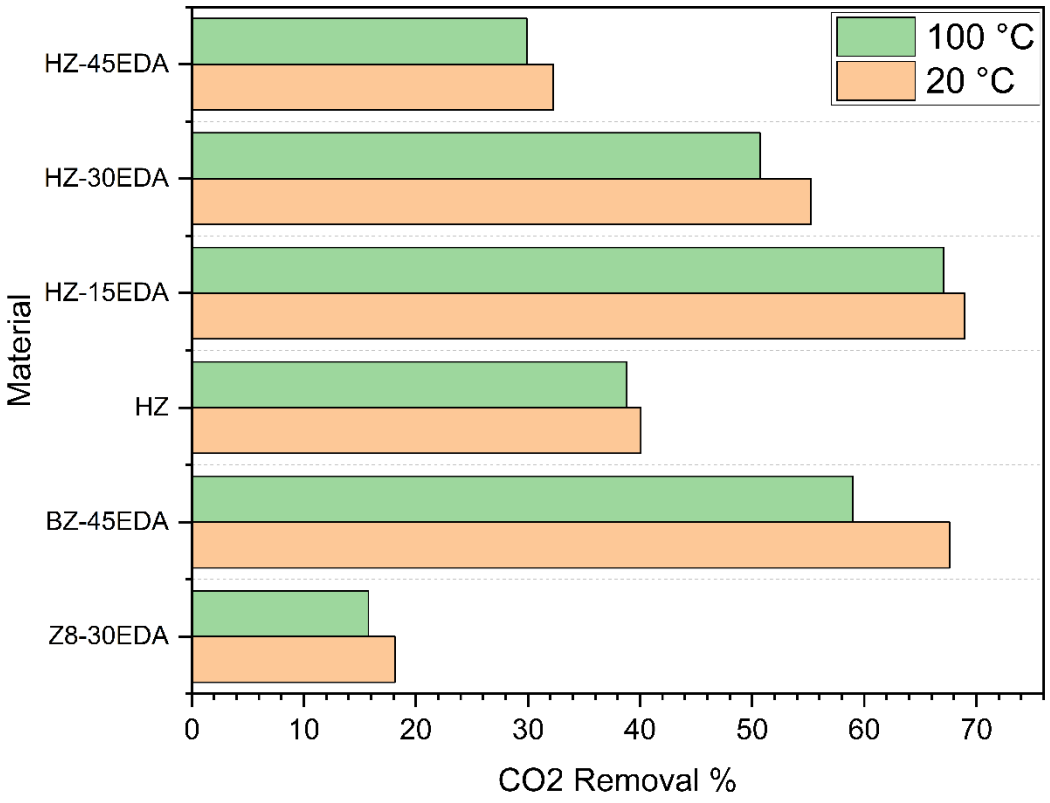

Figure 4.15 CO_2 removal efficiency of selected ZIF materials at 20 °C and 100 °C, highlighting the influence of temperature and amine loading on adsorption behavior

A quantitative comparison of CO_2 removal is presented in Figure 4.15, where an overall decrease in CO_2 removal is observed at elevated temperature for all materials. This trend is expected, as CO_2 adsorption in ZIF-based materials is predominantly exothermic, and increasing temperature reduces adsorption capacity, particularly for physisorption-dominated systems. For Z8-30EDA, CO_2 removal decreases from 18.13% at 20 °C to 15.77% at 100 °C, confirming weak

temperature stability. Similarly, the parent HZ sample shows a slight decrease from 40.07% to 38.83%.

In contrast, BZ-45EDA maintains relatively high performance, with CO_2 removal decreasing from 67.61% to 58.98%, indicating that amine-assisted chemisorption helps retain adsorption capacity at elevated temperature. Among all samples, HZ-15EDA exhibits the best thermal stability, with CO_2 removal decreasing only slightly from 68.94% to 67.08%, suggesting an optimal balance between physisorption and chemisorption. However, higher amine loadings lead to more pronounced reductions, with HZ-30EDA decreasing from 55.24% to 50.72% and HZ-45EDA from 32.28% to 29.93%.

These results can be explained by the temperature dependence of both physisorption and chemisorption. In ZIF-based materials, CO_2, CH_4, and He are primarily adsorbed through exothermic physisorption, so increasing temperature weakens these interactions and reduces uptake. The introduction of EDA adds a chemisorption component through CO_2 amine interactions, which enhances adsorption at lower temperatures but is also sensitive to heating. As temperature increases, these stronger CO_2 amine interactions are destabilized, and equilibrium shifts toward the gas phase, leading to a reduction in CO_2 capacity. This effect is more pronounced at higher amine loadings, where a larger fraction of adsorption relies on specific amine sites that lose occupancy more rapidly with temperature.

As a result, CO_2 selective adsorption over CH_4 and He is still maintained at elevated temperature due to stronger interactions with amine-functionalized sites, but the overall performance declines. BZ-45EDA and HZ-15EDA retain higher performance because their balanced structure allows both sufficient pore accessibility and stable adsorption sites. In contrast,

Z8-30EDA and pristine HZ exhibit weaker adsorption dominated by physisorption, while higher amine loading further reduces performance due to pore blockage, diffusion limitations, and increased temperature sensitivity of chemisorbed species.

4.7 Regeneration and Cyclic Stability

The regeneration and cyclic stability of the synthesized ZIF materials were evaluated over seven consecutive adsorption-desorption cycles (A1-A7), where A1 represents the first adsorption cycle, followed by A2, A3, and so on up to A7. This analysis was performed to assess the reusability of the materials for CO_2 capture applications. The corresponding CO_2 adsorption capacities are presented in Figure 4.16.

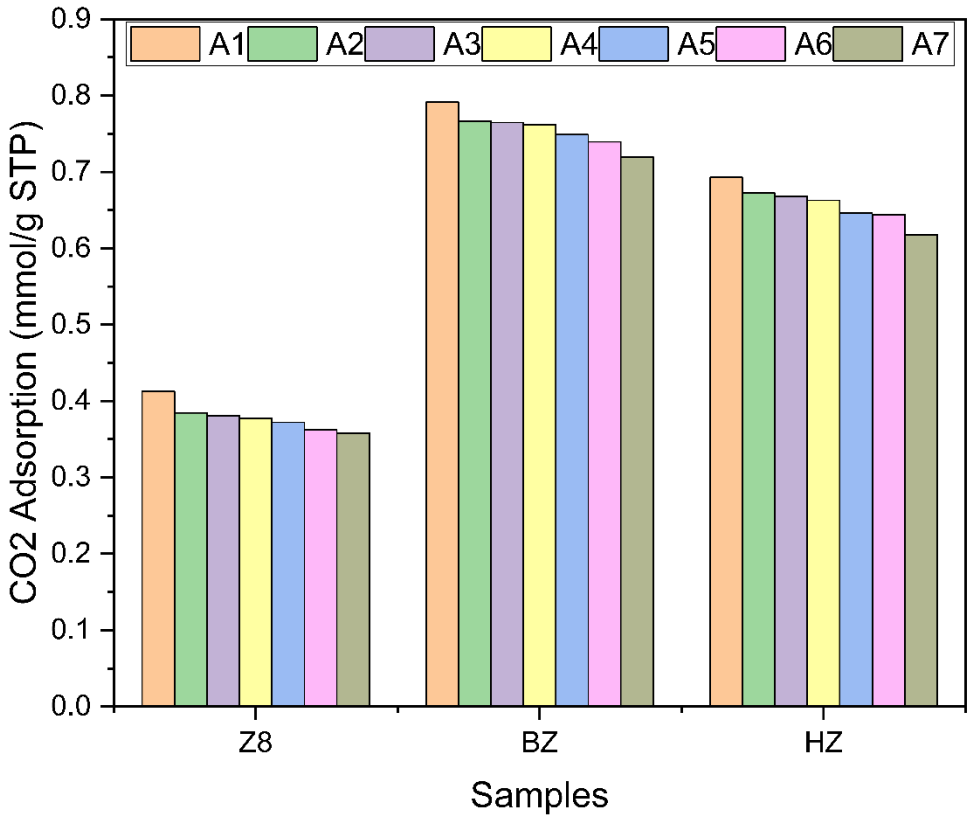

Figure 4.16 Regeneration and cyclic stability of Z8, BZ, and HZ over seven CO_2 adsorption-desorption cycles.

As shown in Figure 4.16, all materials exhibit a gradual decrease in CO_2 adsorption capacity with increasing cycle number, indicating some degree of performance loss during repeated use. For ZIF-8 (Z8), the adsorption decreases from 0.4127 mmol g^{-1} (A1) to 0.3582 mmol g^{-1} (A7), showing a noticeable reduction. This behavior is mainly attributed to its physisorption-dominated mechanism, where weaker interactions are more susceptible to performance loss during repeated cycling.

In contrast, bimetallic ZIF (BZ) demonstrates relatively stable performance, with adsorption decreasing slightly from 0.7912 mmol g^{-1} (A1) to 0.7196 mmol g^{-1} (A7). The smaller reduction indicates better structural robustness and stronger adsorption interactions, likely due to a combination of framework stability and partial chemisorption effects. Similarly, HE-ZIF (HZ) shows moderate stability, with CO_2 adsorption decreasing from 0.6929 mmol g^{-1} (A1) to 0.6177 mmol g^{-1} (A7). Although a decline is observed, the material retains a significant portion of its adsorption capacity, suggesting improved resistance to degradation compared to ZIF-8.

The gradual decrease in adsorption capacity across cycles can be attributed to several factors. Incomplete desorption may leave a small fraction of CO_2 trapped in narrow pores or strong adsorption sites, effectively blocking them in subsequent cycles. Repeated heating and cooling during regeneration can also induce minor structural changes, such as partial loss of micropore volume, slight alterations in the coordination environment, or microstructural damage such as particle fracture and pore collapse. Over multiple cycles, even small reductions in accessible pore volume can cumulatively decrease adsorption capacity.

However, the relatively small loss observed in BZ and HZ samples indicates good regenerability and cyclic stability, highlighting the advantage of more robust frameworks and

stronger adsorption interactions in maintaining performance over repeated adsorption–desorption cycles.

Chapter 5 - Conclusions

This study investigated the synthesis, functionalization, and performance of high-entropy ZIF (HE-ZIF) materials for CO_2 capture. Mechanochemical synthesis was shown to be an effective method, with milling time significantly influencing crystallinity and performance, where the 60-minute milled sample provided optimal results. Amine functionalization with ethylenediamine (EDA) revealed that CO_2 adsorption is governed by a balance between physisorption and chemisorption. Moderate amine loading enhanced CO_2 uptake and selectivity, while higher loading led to pore blockage and reduced accessibility, highlighting the importance of optimization. Comparison among materials showed that bimetallic ZIF exhibits the most stable and consistent performance, whereas HE-ZIF demonstrates superior performance when optimally functionalized (HZ-15EDA). Temperature studies confirmed that adsorption decreases at elevated temperature due to reduced physisorption, while chemisorption helps maintain selectivity in amine-functionalized samples. Regeneration results further indicated good reusability, particularly for bimetallic and HE-ZIF materials. Overall, this work highlights the importance of tuning both framework composition and functionalization to achieve efficient CO_2 capture. Optimized amine-functionalized HE-ZIF materials show strong potential for selective CO_2 adsorption, especially under elevated temperature conditions.

Chapter 6 - References

[1] Cheng W, Dan L, Deng X, Feng J, Wang Y, Peng J, et al. Global monthly gridded atmospheric carbon dioxide concentrations under the historical and future scenarios. Sci Data 2022;9:83. https://doi.org/10.1038/s41597-022-01196-7.

[2] Solaymani S, Botero J. Reducing Carbon Emissions from Transport Sector: Experience and Policy Design Considerations. Sustainability 2025;17:3762. https://doi.org/10.3390/su17093762.

[3] Gür TM. Carbon Dioxide Emissions, Capture, Storage and Utilization: Review of Materials, Processes and Technologies. Prog Energy Combust Sci 2022;89:100965. https://doi.org/10.1016/j.pecs.2021.100965.

[4] Nunes LJR. The Rising Threat of Atmospheric CO2: A Review on the Causes, Impacts, and Mitigation Strategies. Environments 2023;10:66. https://doi.org/10.3390/environments10040066.

[5] Gillett NP, Kirchmeier-Young M, Ribes A, Shiogama H, Hegerl GC, Knutti R, et al. Constraining human contributions to observed warming since the pre-industrial period. Nat Clim Chang 2021;11:207–12. https://doi.org/10.1038/s41558-020-00965-9.

[6] Armstrong McKay DI, Staal A, Abrams JF, Winkelmann R, Sakschewski B, Loriani S, et al. Exceeding 1.5°C global warming could trigger multiple climate tipping points. Science (1979) 2022;377. https://doi.org/10.1126/science.abn7950.

[7] McCulloch MT, Winter A, Sherman CE, Trotter JA. 300 years of sclerosponge thermometry shows global warming has exceeded 1.5 °C. Nat Clim Chang 2024;14:171–7. https://doi.org/10.1038/s41558-023-01919-7.

[8] Meng F, Meng Y, Ju T, Han S, Lin L, Jiang J. Research progress of aqueous amine solution for CO2 capture: A review. Renewable and Sustainable Energy Reviews 2022;168:112902. https://doi.org/10.1016/j.rser.2022.112902.

[9] de Meyer F, Bignaud C. The use of catalysis for faster CO2 absorption and energy-efficient solvent regeneration: An industry-focused critical review. Chemical Engineering Journal 2022;428:131264. https://doi.org/10.1016/j.cej.2021.131264.

[10] Nwaoha C, Supap T, Idem R, Saiwan C, Tontiwachwuthikul P, AL-Marri MJ, et al. Advancement and new perspectives of using formulated reactive amine blends for post-combustion carbon dioxide (CO2) capture technologies. Petroleum 2017;3:10–36. https://doi.org/10.1016/j.petlm.2016.11.002.

[11] Li G, Shen X, Jiao X, Xie F, Hua J, Lin H, et al. Novel tri-solvent amines absorption for flue gas CO2 capture: Efficient absorption and regeneration with low energy consumption. Chemical Engineering Journal 2024;493:152699. https://doi.org/10.1016/j.cej.2024.152699.

[12] Nwaoha C, Supap T, Idem R, Saiwan C, Tontiwachwuthikul P, AL-Marri MJ, et al. Advancement and new perspectives of using formulated reactive amine blends for post-combustion carbon dioxide (CO2) capture technologies. Petroleum 2017;3:10–36. https://doi.org/10.1016/j.petlm.2016.11.002.

[13] Zeng H, Qu X, Xu D, Luo Y. Porous Adsorption Materials for Carbon Dioxide Capture in Industrial Flue Gas. Front Chem 2022;10. https://doi.org/10.3389/fchem.2022.939701.

[14] Gunawardene OHP, Gunathilake CA, Vikrant K, Amaraweera SM. Carbon Dioxide Capture through Physical and Chemical Adsorption Using Porous Carbon Materials: A Review. Atmosphere (Basel) 2022;13:397. https://doi.org/10.3390/atmos13030397.

[15] Liu R, Shi X, Wang C, Gao Y, Xu S, Hao G, et al. Advances in Post-Combustion CO_2 Capture by Physical Adsorption: From Materials Innovation to Separation Practice. ChemSusChem 2021;14:1428–71. https://doi.org/10.1002/cssc.202002677.

[16] Singh R, Wang L, Ostrikov K (Ken), Huang J. Designing Carbon-Based Porous Materials for Carbon Dioxide Capture. Adv Mater Interfaces 2024;11. https://doi.org/10.1002/admi.202202290.

[17] Ding M, Flaig RW, Jiang H-L, Yaghi OM. Carbon capture and conversion using metal–organic frameworks and MOF-based materials. Chem Soc Rev 2019;48:2783–828. https://doi.org/10.1039/C8CS00829A.

[18] Kong F, Chen W. Carbon Dioxide Capture and Conversion Using Metal–Organic Framework (MOF) Materials: A Comprehensive Review. Nanomaterials 2024;14:1340. https://doi.org/10.3390/nano14161340.

[19] Ghanbari T, Abnisa F, Wan Daud WMA. A review on production of metal organic frameworks (MOF) for CO2 adsorption. Science of The Total Environment 2020;707:135090. https://doi.org/10.1016/j.scitotenv.2019.135090.

[20] Li L, Jung HS, Lee JW, Kang YT. Review on applications of metal–organic frameworks for CO2 capture and the performance enhancement mechanisms. Renewable and Sustainable Energy Reviews 2022;162:112441. https://doi.org/10.1016/j.rser.2022.112441.

[21] Yu J, Qi K, Li X, Gao L, Wang J, Zeng J, et al. Insights into zeolite imidazole frameworks (ZIFs) for CO2 capture and separation: A short review. Journal of Environmental Sciences 2025;157:690–709. https://doi.org/10.1016/j.jes.2024.12.002.

[22] Kong F, Chen W. Carbon Dioxide Capture and Conversion Using Metal–Organic Framework (MOF) Materials: A Comprehensive Review. Nanomaterials 2024;14:1340. https://doi.org/10.3390/nano14161340.

[23] Li L, Jung HS, Lee JW, Kang YT. Review on applications of metal–organic frameworks for CO2 capture and the performance enhancement mechanisms. Renewable and Sustainable Energy Reviews 2022;162:112441. https://doi.org/10.1016/j.rser.2022.112441.

[24] Liu J, Thallapally PK, McGrail BP, Brown DR, Liu J. Progress in adsorption-based CO_2 capture by metal–organic frameworks. Chem Soc Rev 2012;41:2308–22. https://doi.org/10.1039/C1CS15221A.

[25] Singh A, Vedrtnam A, Kalauni K, Singh A, Wdowin M. Synthesis routes of zeolitic imidazolate framework-8 for CO_2 capture: A review. AIMS Mater Sci 2025;12:118–64. https://doi.org/10.3934/matersci.2025009.

[26] Tao YR, Zhang GH, Xu HJ. Grand canonical Monte Carlo (GCMC) study on adsorption performance of metal organic frameworks (MOFs) for carbon capture. Sustainable

Materials and Technologies 2022;32:e00383. https://doi.org/10.1016/j.susmat.2021.e00383.

[27] Ngoc Son D, Chihaia V, Thi Xuan Huynh N. Efficiency of carbon dioxide capture with metal substitutions in the MIL-88A metal–organic framework. RSC Adv 2025;15:1425–37. https://doi.org/10.1039/D4RA07861F.

[28] Do HH, Rabani I, Truong HB. Metal-organic framework-based nanomaterials for CO_2 storage: A review. Beilstein Journal of Nanotechnology 2023;14:964–70. https://doi.org/10.3762/bjnano.14.79.

[29] Sikma RE, Vogel DJ, Reyes RA, Meyerson ML, Kotula PG, Gallis DFS. High-Entropy Metal-Organic Frameworks (HEMOFs): A New Frontier in Materials Design for CO_2 Utilization. Advanced Materials 2024;36. https://doi.org/10.1002/adma.202407435.

[30] Ye L, Zhang Y, Jin S, Zhou C, Pang J, Luo Y, et al. Mechanochemical Synthesis of High-Entropy MOF-74 with Multiple Active Sites for CO_2 Adsorption and Synergistic Conversion. Inorg Chem 2024;63:20572–83. https://doi.org/10.1021/acs.inorgchem.4c03228.

[31] Wu S-C, Chang P-H, Lin C-Y, Peng C-H. Multi-Metals CaMgAl Metal-Organic Framework as CaO-based Sorbent to Achieve Highly CO2 Capture Capacity and Cyclic Performance. Materials 2020;13:2220. https://doi.org/10.3390/ma13102220.

[32] Rahim AHA, Hamidon NF, Yunus NM, Bustam MA, Aziz SFNA, Jumbri K, et al. Unveiling the Potential of Room-Temperature Synthesis of a Mixed-Linker Zeolitic

Imidazolate Framework-76 for CO2 Capture. Processes 2025;13:320. https://doi.org/10.3390/pr13020320.

[33] Mehri Lighvan Z, Hosseini SR, Norouzbahari S, Sadatnia B, Ghadimi A. Synthesis, characterization, and selective gas adsorption performance of hybrid NH2-MIL-101(Fe)/ZIF-8 metal organic framework (MOF). Fuel 2023;351:128991. https://doi.org/10.1016/j.fuel.2023.128991.

[34] Sardar P, Bhattacharya G, Manna R, Raj S, Rahut S, Nath Samanta A. Excellent CO2 adsorption performance of amine-impregnated highly porous ZIF-8 adsorbent: Experimental and isotherm modeling studies. Advanced Powder Technology 2024;35:104344. https://doi.org/10.1016/j.apt.2024.104344.

[35] Yang H. Simulation of CO_2 adsorption by porous materials based on lattice Boltzmann method. J Phys Conf Ser 2025;2964:012090. https://doi.org/10.1088/1742-6596/2964/1/012090.

[36] Geweda AE, Zayed ME, Khan MY, Alquaity ABS. Mitigating CO2 emissions: A review on emerging technologies/strategies for CO2 capture. Journal of the Energy Institute 2025;118:101911. https://doi.org/10.1016/j.joei.2024.101911.

[37] Fu L, Ren Z, Si W, Ma Q, Huang W, Liao K, et al. Research progress on CO2 capture and utilization technology. Journal of CO2 Utilization 2022;66:102260. https://doi.org/10.1016/j.jcou.2022.102260.

[38] Li H, Li L, Lin R-B, Zhou W, Zhang Z, Xiang S, et al. Porous metal-organic frameworks for gas storage and separation: Status and challenges. EnergyChem 2019;1:100006. https://doi.org/10.1016/j.enchem.2019.100006.

[39] Singh A, Vedrtnam A, Kalauni K, Singh A, Wdowin M. Synthesis routes of zeolitic imidazolate framework-8 for CO_2 capture: A review. AIMS Mater Sci 2025;12:118–64. https://doi.org/10.3934/matersci.2025009.

[40] Pimentel BR, Parulkar A, Zhou E, Brunelli NA, Lively RP. Zeolitic Imidazolate Frameworks: Next-Generation Materials for Energy-Efficient Gas Separations. ChemSusChem 2014;7:3202–40. https://doi.org/10.1002/cssc.201402647.

[41] Yu J, Qi K, Li X, Gao L, Wang J, Zeng J, et al. Insights into zeolite imidazole frameworks (ZIFs) for CO2 capture and separation: A short review. Journal of Environmental Sciences 2025;157:690–709. https://doi.org/10.1016/j.jes.2024.12.002.

[42] Kouser S, Hezam A, Khadri MJN, Khanum SA. A review on zeolite imidazole frameworks: synthesis, properties, and applications. Journal of Porous Materials 2022;29:663–81. https://doi.org/10.1007/s10934-021-01184-z.

[43] Paul A, Banga IK, Muthukumar S, Prasad S. Engineering the ZIF-8 Pore for Electrochemical Sensor Applications─A Mini Review. ACS Omega 2022;7:26993–7003. https://doi.org/10.1021/acsomega.2c00737.

[44] Eltaweil AS, Abd El-Monaem EM, Elshishini HM, El-Aqapa HG, Hosny M, Abdelfatah AM, et al. Recent developments in alginate-based adsorbents for removing phosphate ions

from wastewater: a review. RSC Adv 2022;12:8228–48. https://doi.org/10.1039/D1RA09193J.

[45] Li P, Xu Y, Yin L, Liang X, Wang R, Liu K. Development of Raw Materials and Technology for Pulping—A Brief Review. Polymers (Basel) 2023;15. https://doi.org/10.3390/polym15224465.

[46] Kim JK, Moon YH, Eo SH. Compressive strength development of concrete with different curing time and temperature. Cem Concr Res 1998;28:1761–73. https://doi.org/10.1016/S0008-8846(98)00164-1.

[47] Sandberg C, Hill J, Jackson M. On the development of the refiner mechanical pulping process - A review. Nord Pulp Paper Res J 2020;35. https://doi.org/10.1515/npprj-2019-0083.

[48] Lai Z. Development of ZIF-8 membranes: opportunities and challenges for commercial applications. Curr Opin Chem Eng 2018;20:78–85. https://doi.org/10.1016/j.coche.2018.03.002.

[49] Sardar P, Bhattacharya G, Manna R, Raj S, Rahut S, Nath Samanta A. Excellent CO2 adsorption performance of amine-impregnated highly porous ZIF-8 adsorbent: Experimental and isotherm modeling studies. Advanced Powder Technology 2024;35:104344. https://doi.org/10.1016/j.apt.2024.104344.

[50] Sun Y, Dai S. High-entropy materials for catalysis: A new frontier. Sci Adv 2021;7. https://doi.org/10.1126/sciadv.abg1600.

[51] Xing J, Liu Y, Mathew G, He Q, Aghassi-Hagmann J, Schweidler S, et al. High-Entropy Metal–Organic Frameworks and Their Derivatives: Advances in Design, Synthesis, and Applications for Catalysis and Energy Storage. Advanced Science 2025;12. https://doi.org/10.1002/advs.202411175.

[52] Singh B, Draksharapu A. Recent Progress in Catalysis Using High-Entropy Metal–Organic Frameworks and their Derived Materials. ChemSusChem 2025;18. https://doi.org/10.1002/cssc.202500750.

[53] Nam J, Cho C, Jung S, Jung M, Kim Y, Hong Y, et al. High-Entropy Zeolitic Imidazolate Frameworks for Dynamic Hydrogen Isotope Separation. Angew Chem Int Ed 2025;64. https://doi.org/10.1002/anie.202420379.

[54] Liu Y, Deng C, Wu P, Liu H, Liu F, Liu R, et al. High-entropy zeolitic imidazolate framework for efficient oxidative desulfurization of diesel fuel: Towards complete sulfur removal and valuable sulfone production. Fuel 2024;359:130375. https://doi.org/10.1016/j.fuel.2023.130375.

[55] Xu W, Chen H, Jie K, Yang Z, Li T, Dai S. Entropy-Driven Mechanochemical Synthesis of Polymetallic Zeolitic Imidazolate Frameworks for CO_2 Fixation. Angew Chem Int Ed 2019;58:5018–22. https://doi.org/10.1002/anie.201900787.

[56] Missaoui N, Bouzid M, Chrouda A, Kahri H, Barhoumi H, Pang AL, et al. Interpreting of the carbon dioxide adsorption on high surface area zeolitic imidazolate Framework-8 (ZIF-8) nanoparticles using a statistical physics model. Microporous and Mesoporous Materials 2023;360:112711. https://doi.org/10.1016/j.micromeso.2023.112711.

[57] Khan AU, Noor T, Iqbal N, Zaman N, Hussain Z. CO2 adsorption study of the zeolite imidazolate framework (ZIF-8) and its g-C3N4 composites. J Mater Sci 2023;58:3947–59. https://doi.org/10.1007/s10853-023-08253-5.

[58] Missaoui N, Kahri H, Demirci UB. Rapid room-temperature synthesis and characterizations of high-surface-area nanoparticles of zeolitic imidazolate framework-8 (ZIF-8) for CO2 and CH4 adsorption. J Mater Sci 2022;57:16245–57. https://doi.org/10.1007/s10853-022-07676-w.

[59] Ahmed Khalil S, Missaoui N, Alatawi RAS, Keshk AA, Alatawi O, Albalawi TA, et al. An Ultramicroporous Zinc-Based Zeolitic Imidazolate Framework-8 for the Adsorption of CO $_2$, CH $_4$, CO, N $_2$ and H $_2$: A Combined Experimental and Theoretical Study. ChemistrySelect 2024;9. https://doi.org/10.1002/slct.202402556.

[60] Kouser S, Hezam A, Khadri MJN, Khanum SA. A review on zeolite imidazole frameworks: synthesis, properties, and applications. Journal of Porous Materials 2022;29:663–81. https://doi.org/10.1007/s10934-021-01184-z.

[61] Lee Y-R, Kim J, Ahn W-S. Synthesis of metal-organic frameworks: A mini review. Korean Journal of Chemical Engineering 2013;30:1667–80. https://doi.org/10.1007/s11814-013-0140-6.

[62] Pouramini Z, Mousavi SM, Babapoor A, Hashemi SA, Lai CW, Mazaheri Y, et al. Effect of Metal Atom in Zeolitic Imidazolate Frameworks (ZIF-8 & 67) for Removal of Dyes and Antibiotics from Wastewater: A Review. Catalysts 2023;13:155. https://doi.org/10.3390/catal13010155.

[63] Pouramini Z, Mousavi SM, Babapoor A, Hashemi SA, Lai CW, Mazaheri Y, et al. Effect of Metal Atom in Zeolitic Imidazolate Frameworks (ZIF-8 & 67) for Removal of Dyes and Antibiotics from Wastewater: A Review. Catalysts 2023;13:155. https://doi.org/10.3390/catal13010155.

[64] Bhattacharjee S, Jang M-S, Kwon H-J, Ahn W-S. Zeolitic Imidazolate Frameworks: Synthesis, Functionalization, and Catalytic/Adsorption Applications. Catalysis Surveys from Asia 2014;18:101–27. https://doi.org/10.1007/s10563-014-9169-8.

[65] Lee T, Kim H, Cho W, Han D-Y, Ridwan M, Yoon CW, et al. Thermosensitive Structural Changes and Adsorption Properties of Zeolitic Imidazolate Framework-8 (ZIF-8). The Journal of Physical Chemistry C 2015;119:8226–37. https://doi.org/10.1021/acs.jpcc.5b01519.

[66] Hurlock MJ, Christian MS, Fritzsching KJ, Rademacher DX, Rimsza JM, Nenoff TM. Experimental and Computational Mechanisms that Govern Long-Term Stability of CO_2-Adsorbed ZIF-8-Based Porous Liquids. ACS Appl Mater Interfaces 2023;15:32792–802. https://doi.org/10.1021/acsami.3c06177.

[67] Mohamedali M, Ibrahim H, Henni A. Incorporation of acetate-based ionic liquids into a zeolitic imidazolate framework (ZIF-8) as efficient sorbents for carbon dioxide capture. Chemical Engineering Journal 2018;334:817–28. https://doi.org/10.1016/j.cej.2017.10.104.

[68] Wang N, Wang D, Krook-Riekkola A, Ji X. MEA-based CO2 capture: a study focuses on MEA concentrations and process parameters. Front Energy Res 2023;11. https://doi.org/10.3389/fenrg.2023.1230743.

[69] Abu-Zahra MRM, Schneiders LHJ, Niederer JPM, Feron PHM, Versteeg GF. CO2 capture from power plants. International Journal of Greenhouse Gas Control 2007;1:37–46. https://doi.org/10.1016/S1750-5836(06)00007-7.

[70] Vinjarapu SHB, Neerup R, Larsen AH, Jørsboe JK, Villadsen SNB, Jensen S, et al. Results from pilot-scale CO <math altimg="si60.svg" display="inline" id="d1e18243"> <msub> <mrow/> <mrow> <mn>2</mn> </mrow> </msub> </math> capture testing using 30 wt% MEA at a Waste-to-Energy facility: Optimisation through parametric analysis. Appl Energy 2024;355:122193. https://doi.org/10.1016/j.apenergy.2023.122193.

[71] Sai Bhargava Reddy M, Ponnamma D, Sadasivuni KK, Kumar B, Abdullah AM. Carbon dioxide adsorption based on porous materials. RSC Adv 2021;11:12658–81. https://doi.org/10.1039/D0RA10902A.

[72] Kim KH, Kim MH. Adsorption of CO2, CO, H2, and N2 on Zeolites, Activated Carbons, and Metal-Organic Frameworks with Different Surface Nonuniformities. Sustainability 2023;15:11574. https://doi.org/10.3390/su151511574.

[73] Głowniak S, Szczęśniak B, Choma J, Jaroniec M. Mechanochemical Synthesis of MOF-303 and Its CO2 Adsorption at Ambient Conditions. Molecules 2024;29:2698. https://doi.org/10.3390/molecules29112698.

[74] Zhao G, Li Z, Cheng B, Zhuang X, Lin T. Hierarchical porous metal organic framework aerogel for highly efficient CO2 adsorption. Sep Purif Technol 2023;315:123754. https://doi.org/10.1016/j.seppur.2023.123754.

[75] Kazemi A, Pordsari MA, Tamtaji M, Afshari MH, Keshavarz S, Zeinali F, et al. Unveiling the power of defect engineering in MOF-808 to enhance efficient carbon dioxide adsorption and separation by harnessing the potential of DFT analysis. Chemical Engineering Journal 2024;494:153049. https://doi.org/10.1016/j.cej.2024.153049.

[76] Park JW, Heo S, Yeo J-G, Lee S, Kim J-K, Lee JH. Membrane-Based CO2 Capture Across Industrial Sectors: Process Conditions, Case Studies, and Implementation Insights. Membranes (Basel) 2025;15:200. https://doi.org/10.3390/membranes15070200.

[77] Han Y, Ho WSW. Polymeric membranes for CO2 separation and capture. J Memb Sci 2021;628:119244. https://doi.org/10.1016/j.memsci.2021.119244.

[78] Checchetto R, De Angelis MG, Minelli M. Exploring the membrane-based separation of CO2/CO mixtures for CO2 capture and utilisation processes: Challenges and opportunities. Sep Purif Technol 2024;346:127401. https://doi.org/10.1016/j.seppur.2024.127401.

[79] Lasseuguette E, Carta M, Brandani S, Ferrari M-C. Effect of humidity and flue gas impurities on CO2 permeation of a polymer of intrinsic microporosity for post-combustion capture. International Journal of Greenhouse Gas Control 2016;50:93–9. https://doi.org/10.1016/j.ijggc.2016.04.023.

[80] Shen M, Tong L, Yin S, Liu C, Wang L, Feng W, et al. Cryogenic technology progress for CO2 capture under carbon neutrality goals: A review. Sep Purif Technol 2022;299:121734. https://doi.org/10.1016/j.seppur.2022.121734.

[81] Aneesh AM, Sam AA. A mini-review on cryogenic carbon capture technology by desublimation: theoretical and modeling aspects. Front Energy Res 2023;11. https://doi.org/10.3389/fenrg.2023.1167099.

[82] Xu G, Liang F, Yang Y, Hu Y, Zhang K, Liu W. An Improved CO2 Separation and Purification System Based on Cryogenic Separation and Distillation Theory. Energies (Basel) 2014;7:3484–502. https://doi.org/10.3390/en7053484.

[83] Sarwar A, Ali M, Khoja AH, Nawar A, Waqas A, Liaquat R, et al. Synthesis and characterization of biomass-derived surface-modified activated carbon for enhanced CO2 adsorption. Journal of CO2 Utilization 2021;46:101476. https://doi.org/10.1016/j.jcou.2021.101476.

[84] Gautam, Sahoo S. Experimental investigation on different activated carbons as adsorbents for CO2 capture. Thermal Science and Engineering Progress 2022;33:101339. https://doi.org/10.1016/j.tsep.2022.101339.

[85] Gautam, Sahoo S. Experimental investigation on different activated carbons as adsorbents for CO2 capture. Thermal Science and Engineering Progress 2022;33:101339. https://doi.org/10.1016/j.tsep.2022.101339.

[86] Boer DG, Langerak J, Pescarmona PP. Zeolites as Selective Adsorbents for CO_2 Separation. ACS Appl Energy Mater 2023;6:2634–56. https://doi.org/10.1021/acsaem.2c03605.

[87] Yang X, Wang Q, Chen J, Liu H, Xu L, Rao M. Competitive Adsorption of Moisture and SO2 for Carbon Dioxide Capture by Zeolites FAU 13X and LTA 5A. Processes 2024;12:1547. https://doi.org/10.3390/pr12081547.

[88] Bae JY, Jang SG, Cho J, Kang M. Amine-Functionalized Mesoporous Silica for Efficient CO2 Capture: Stability, Performance, and Industrial Feasibility. Int J Mol Sci 2025;26:4313. https://doi.org/10.3390/ijms26094313.

[89] Chang F-Y, Chao K-J, Cheng H-H, Tan C-S. Adsorption of CO2 onto amine-grafted mesoporous silicas. Sep Purif Technol 2009;70:87–95. https://doi.org/10.1016/j.seppur.2009.08.016.

[90] Chang F-Y, Chao K-J, Cheng H-H, Tan C-S. Adsorption of CO2 onto amine-grafted mesoporous silicas. Sep Purif Technol 2009;70:87–95. https://doi.org/10.1016/j.seppur.2009.08.016.

[91] Henao W, Jaramillo LY, López D, Romero-Sáez M, Buitrago-Sierra R. Insights into the CO2 capture over amine-functionalized mesoporous silica adsorbents derived from rice husk ash. J Environ Chem Eng 2020;8:104362. https://doi.org/10.1016/j.jece.2020.104362.

[92] Bae JY, Jang SG, Cho J, Kang M. Amine-Functionalized Mesoporous Silica for Efficient CO2 Capture: Stability, Performance, and Industrial Feasibility. Int J Mol Sci 2025;26:4313. https://doi.org/10.3390/ijms26094313.

[93] Hack J, Maeda N, Meier DM. Review on CO $_2$ Capture Using Amine-Functionalized Materials. ACS Omega 2022;7:39520–30. https://doi.org/10.1021/acsomega.2c03385.

[94] Chang F-Y, Chao K-J, Cheng H-H, Tan C-S. Adsorption of CO2 onto amine-grafted mesoporous silicas. Sep Purif Technol 2009;70:87–95. https://doi.org/10.1016/j.seppur.2009.08.016.

[95] Ünveren EE, Monkul BÖ, Sarıoğlan Ş, Karademir N, Alper E. Solid amine sorbents for CO2 capture by chemical adsorption: A review. Petroleum 2017;3:37–50. https://doi.org/10.1016/j.petlm.2016.11.001.

[96] Darunte LA, Walton KS, Sholl DS, Jones CW. CO2 capture via adsorption in amine-functionalized sorbents. Curr Opin Chem Eng 2016;12:82–90. https://doi.org/10.1016/j.coche.2016.03.002.

[97] Dziejarski B, Serafin J, Andersson K, Krzyżyńska R. CO2 capture materials: a review of current trends and future challenges. Materials Today Sustainability 2023;24:100483. https://doi.org/10.1016/j.mtsust.2023.100483.

[98] Zhou D-D, Zhang X-W, Mo Z-W, Xu Y-Z, Tian X-Y, Li Y, et al. Adsorptive separation of carbon dioxide: From conventional porous materials to metal–organic frameworks. EnergyChem 2019;1:100016. https://doi.org/10.1016/j.enchem.2019.100016.

[99] Boer DG, Langerak J, Pescarmona PP. Zeolites as Selective Adsorbents for CO_2 Separation. ACS Appl Energy Mater 2023;6:2634–56. https://doi.org/10.1021/acsaem.2c03605.

[100] Dziejarski B, Serafin J, Andersson K, Krzyżyńska R. CO2 capture materials: a review of current trends and future challenges. Materials Today Sustainability 2023;24:100483. https://doi.org/10.1016/j.mtsust.2023.100483.

[101] Mahajan S, Lahtinen M. Recent progress in metal-organic frameworks (MOFs) for CO2 capture at different pressures. J Environ Chem Eng 2022;10:108930. https://doi.org/10.1016/j.jece.2022.108930.

[102] Gebremariam SK, Varghese AM, Ehrling S, Al Wahedi Y, AlHajaj A, Dumée LF, et al. Hierarchically Porous Structured Adsorbents with Ultrahigh Metal–Organic Framework Loading for CO_2 Capture. ACS Appl Mater Interfaces 2024;16:50785–99. https://doi.org/10.1021/acsami.4c10730.

[103] Phan A, Doonan CJ, Uribe-Romo FJ, Knobler CB, O'Keeffe M, Yaghi OM. Synthesis, Structure, and Carbon Dioxide Capture Properties of Zeolitic Imidazolate Frameworks. Acc Chem Res 2010;43:58–67. https://doi.org/10.1021/ar900116g.

[104] Park KS, Ni Z, Côté AP, Choi JY, Huang R, Uribe-Romo FJ, et al. Exceptional chemical and thermal stability of zeolitic imidazolate frameworks. Proceedings of the National Academy of Sciences 2006;103:10186–91. https://doi.org/10.1073/pnas.0602439103.

[105] Butt FS, Lewis A, Rea R, Mazlan NA, Chen T, Radacsi N, et al. Highly-Controlled Soft-Templating Synthesis of Hollow ZIF-8 Nanospheres for Selective CO_2 Separation and Storage. ACS Appl Mater Interfaces 2023;15:31740–54. https://doi.org/10.1021/acsami.3c06502.

[106] Yin X, An T, Wang Y, Zhang L. A novel 3D metal organic framework based on an Azolate ligand. Chem Res Chin Univ 2014;30:1–3. https://doi.org/10.1007/s40242-014-3501-8.

[107] Belgacem CH, Missaoui N, Khalafalla MAH, Bouzid G, Kahri H, Bashal AH, et al. Synthesis of ultramicroporous zeolitic imidazolate framework ZIF-8 via solid state method using a minimum amount of deionized water for high greenhouse gas adsorption: A computational modeling. J Environ Chem Eng 2024;12:112086. https://doi.org/10.1016/j.jece.2024.112086.

[108] Izzaouihda S, Abou El Makarim H, Benoit DM, Komiha N. Theoretical Study of the CO_2 Adsorption by Zeolitic Imidazolate Frameworks (ZIFs). The Journal of Physical Chemistry C 2017;121:20259–65. https://doi.org/10.1021/acs.jpcc.7b04977.

[109] Chiang Y-C, Chin W-T. Preparation of Zeolitic Imidazolate Framework-8-Based Nanofiber Composites for Carbon Dioxide Adsorption. Nanomaterials 2022;12:1492. https://doi.org/10.3390/nano12091492.

[110] Paudel HP, Shi W, Hopkinson D, Steckel JA, Duan Y. Computational modelling of adsorption and diffusion properties of CO_2 and CH_4 in ZIF-8 for gas separation applications: a density functional theory approach. React Chem Eng 2021;6:990–1001. https://doi.org/10.1039/D0RE00416B.

[111] Jiang S, Liu J, Guan J, Du X, Chen S, Song Y, et al. Enhancing CO2 adsorption capacity of ZIF-8 by synergetic effect of high pressure and temperature. Sci Rep 2023;13:17584. https://doi.org/10.1038/s41598-023-44960-4.

[112] Chiang Y-C, Chin W-T. Preparation of Zeolitic Imidazolate Framework-8-Based Nanofiber Composites for Carbon Dioxide Adsorption. Nanomaterials 2022;12:1492. https://doi.org/10.3390/nano12091492.

[113] Liu D, Zheng C, Yang Q, Zhong C. Understanding the Adsorption and Diffusion of Carbon Dioxide in Zeolitic Imidazolate Frameworks: A Molecular Simulation Study. The Journal of Physical Chemistry C 2009;113:5004–9. https://doi.org/10.1021/jp809373r.

[114] Amrouche H, Aguado S, Pérez-Pellitero J, Chizallet C, Siperstein F, Farrusseng D, et al. Experimental and Computational Study of Functionality Impact on Sodalite–Zeolitic Imidazolate Frameworks for CO_2 Separation. The Journal of Physical Chemistry C 2011;115:16425–32. https://doi.org/10.1021/jp202804g.

[115] Åhlén M, Jaworski A, Strømme M, Cheung O. Selective adsorption of CO2 and SF6 on mixed-linker ZIF-7–8s: The effect of linker substitution on uptake capacity and kinetics. Chemical Engineering Journal 2021;422:130117. https://doi.org/10.1016/j.cej.2021.130117.

[116] Li M, Liu J, Deng S, Liu Q, Qi N, Chen Z. Low-Pressure CO_2 Capture in Zeolite Imidazole Frameworks with Ultramicropores Studied by Positron Annihilation. ACS Appl Energy Mater 2021;4:7983–91. https://doi.org/10.1021/acsaem.1c01297.

[117] Atchutha Rao P, Padhy H, Venkateswara Rao A, Kumar Ganta R, Bevara S, Maddila S, et al. Facile synthesis of benzimidazole based mono- and bimetallic zeolitic imidazole frameworks for enhanced CO2 capture performance. Inorg Chem Commun 2024;165:112576. https://doi.org/10.1016/j.inoche.2024.112576.

[118] Zhou K, Mousavi B, Luo Z, Phatanasri S, Chaemchuen S, Verpoort F. Characterization and properties of Zn/Co zeolitic imidazolate frameworks vs. ZIF-8 and ZIF-67. J Mater Chem A Mater 2017;5:952–7. https://doi.org/10.1039/C6TA07860E.

[119] Nandigama SK, Bheeram VR, Mukkamala SB. Rapid synthesis of mono/bimetallic (Zn/Co/Zn–Co) zeolitic imidazolate frameworks at room temperature and evolution of their CO2 uptake capacity. Environ Chem Lett 2019;17:447–54. https://doi.org/10.1007/s10311-018-0775-y.

[120] Sun Y, Dai S. High-entropy materials for catalysis: A new frontier. Sci Adv 2021;7. https://doi.org/10.1126/sciadv.abg1600.

[121] Ren J, Kumkale VY, Hou H, Kadam VS, Jagtap C V., Lokhande PE, et al. A review of high-entropy materials with their unique applications. Adv Compos Hybrid Mater 2025;8:195. https://doi.org/10.1007/s42114-025-01275-4.

[122] Aamlid SS, Oudah M, Rottler J, Hallas AM. Understanding the Role of Entropy in High Entropy Oxides. J Am Chem Soc 2023;145:5991–6006. https://doi.org/10.1021/jacs.2c11608.

[123] Fracchia M, Coduri M, Manzoli M, Ghigna P, Tamburini UA. Is configurational entropy the main stabilizing term in rock-salt Mg0.2Co0.2Ni0.2Cu0.2Zn0.2O high entropy oxide? Nat Commun 2022;13:2977. https://doi.org/10.1038/s41467-022-30674-0.

[124] Xu W, Chen H, Jie K, Yang Z, Li T, Dai S. Entropy-Driven Mechanochemical Synthesis of Polymetallic Zeolitic Imidazolate Frameworks for CO_2 Fixation. Angew Chem Int Ed 2019;58:5018–22. https://doi.org/10.1002/anie.201900787.

[125] Xu W, Chen H, Jie K, Yang Z, Li T, Dai S. Entropy-Driven Mechanochemical Synthesis of Polymetallic Zeolitic Imidazolate Frameworks for CO_2 Fixation. Angew Chem Int Ed 2019;58:5018–22. https://doi.org/10.1002/anie.201900787.

[126] James JB, Lin YS. Kinetics of ZIF-8 Thermal Decomposition in Inert, Oxidizing, and Reducing Environments. The Journal of Physical Chemistry C 2016;120:14015–26. https://doi.org/10.1021/acs.jpcc.6b01208.

[127] Hou S, Ma X, Shu Y, Bao J, Zhang Q, Chen M, et al. Self-regeneration of supported transition metals by a high entropy-driven principle. Nat Commun 2021;12:5917. https://doi.org/10.1038/s41467-021-26160-8.

[128] Rim G, Priyadarshini P, Song M, Wang Y, Bai A, Realff MJ, et al. Support Pore Structure and Composition Strongly Influence the Direct Air Capture of CO_2 on Supported Amines. J Am Chem Soc 2023;145:7190–204. https://doi.org/10.1021/jacs.2c12707.

[129] Hahn MW, Jelic J, Berger E, Reuter K, Jentys A, Lercher JA. Role of Amine Functionality for CO_2 Chemisorption on Silica. J Phys Chem B 2016;120:1988–95. https://doi.org/10.1021/acs.jpcb.5b10012.

[130] Yu J, Chuang SSC. The Structure of Adsorbed Species on Immobilized Amines in CO_2 Capture: An in Situ IR Study. Energy & Fuels 2016;30:7579–87. https://doi.org/10.1021/acs.energyfuels.6b01423.

[131] Lee G, Jhung SH. CO2 capture using functionalized MIL-101(Cr) metal–organic frameworks: Functionality nanoarchitectonics of nanospace for CO2 adsorption. Sep Purif Technol 2025;354:129514. https://doi.org/10.1016/j.seppur.2024.129514.

[132] Hack J, Maeda N, Meier DM. Review on CO_2 Capture Using Amine-Functionalized Materials. ACS Omega 2022;7:39520–30. https://doi.org/10.1021/acsomega.2c03385.

[133] Wang S, Wang S, Zhuo Y. The comparison of regeneration energy of different solid adsorbents in temperature swing adsorption process: A review. Adsorption Science & Technology 2025;43. https://doi.org/10.1177/02636174251385608.

[134] Guta YA, Carneiro J, Li S, Innocenti G, Pang SH, Sakwa-Novak MA, et al. Contributions of CO_2 , O_2 , and H_2O to the Oxidative Stability of Solid Amine Direct Air Capture Sorbents at Intermediate Temperature. ACS Appl Mater Interfaces 2023;15:46790–802. https://doi.org/10.1021/acsami.3c08140.

[135] Yang Y, Shin YK, Ooe H, Hasegawa U, Yamane S, Yamada H, et al. Adsorption of CO_2 by Amine-Functionalized Metal–Organic Frameworks Using GCMC and ReaxFF-Based

Metadynamics Simulations. The Journal of Physical Chemistry C 2024;128:5257–70. https://doi.org/10.1021/acs.jpcc.3c07183.

[136] Zhao S, Zhang Y, Li L, Feng J, Qiu W, Ning Y, et al. Degradation of amine-functionalized adsorbents in carbon capture and direct air capture applications: Mechanism and solutions. Sep Purif Technol 2025;354:129586. https://doi.org/10.1016/j.seppur.2024.129586.

[137] Yu Q, Delgado J de la P, Veneman R, Brilman DWF. Stability of a Benzyl Amine Based CO_2 Capture Adsorbent in View of Regeneration Strategies. Ind Eng Chem Res 2017;56:3259–69. https://doi.org/10.1021/acs.iecr.6b04645.

[138] Jiang S, Liu J, Guan J, Du X, Chen S, Song Y, et al. Enhancing CO2 adsorption capacity of ZIF-8 by synergetic effect of high pressure and temperature. Sci Rep 2023;13:17584. https://doi.org/10.1038/s41598-023-44960-4.

[139] Wang Q, Chen Y, Liu P, Wang Y, Yang J, Li J, et al. CO2 Capture from High-Humidity Flue Gas Using a Stable Metal–Organic Framework. Molecules 2022;27:5608. https://doi.org/10.3390/molecules27175608.

[140] Butt FS, Lewis A, Rea R, Mazlan NA, Chen T, Radacsi N, et al. Highly-Controlled Soft-Templating Synthesis of Hollow ZIF-8 Nanospheres for Selective CO_2 Separation and Storage. ACS Appl Mater Interfaces 2023;15:31740–54. https://doi.org/10.1021/acsami.3c06502.

[141] Kong M, Song L, Liao H, Zhang S, Wang Y, Deng X, et al. A review on development of post-combustion CO2 capture technologies: Performance of carbon-based, zeolites and MOFs adsorbents. Fuel 2024;371:132103. https://doi.org/10.1016/j.fuel.2024.132103.

[142] Missaoui N, Chrouda A, Bourguiba F, Serafin J. Impact of metal precursor and molar ratios on adsorption and separation of CO2 and CH4 by SOD-ZIF-67 prepared using green solvent-free synthesis. Fuel 2024;378:132840. https://doi.org/10.1016/j.fuel.2024.132840.

[143] Głowniak S, Szczęśniak B, Choma J, Jaroniec M. Mechanochemical Synthesis of MOF-303 and Its CO2 Adsorption at Ambient Conditions. Molecules 2024;29:2698. https://doi.org/10.3390/molecules29112698.

[144] Zhang Y, Zhang D, Lei P, Yang Z, Zhang Z. Synthesis of Ca-based metal–organic frameworks from carbide slag for CO2 adsorption. Sep Purif Technol 2024;335:126247. https://doi.org/10.1016/j.seppur.2023.126247.

[145] Van de Voorde B, Stassen I, Bueken B, Vermoortele F, De Vos D, Ameloot R, et al. Improving the mechanical stability of zirconium-based metal–organic frameworks by incorporation of acidic modulators. J Mater Chem A Mater 2015;3:1737–42. https://doi.org/10.1039/C4TA06396A.

[146] Zelenka T, Baláž M, Férová M, Diko P, Bednarčík J, Királyová A, et al. The influence of HKUST-1 and MOF-76 hand grinding/mechanical activation on stability, particle size, textural properties and carbon dioxide sorption. Sci Rep 2024;14:15386. https://doi.org/10.1038/s41598-024-66432-z.

[147] Al Abdulla S, Sabouni R, Ghommem M, Alami AH. Synthesis and performance analysis of zeolitic imidazolate frameworks for CO2 sensing applications. Heliyon 2023;9:e21349. https://doi.org/10.1016/j.heliyon.2023.e21349.

[148] Zhang Z, Li P, Zhao T, Xia Y. Enhanced CO_2 Adsorption and Selectivity of CO_2 /N_2 on Amine@ZIF-8 Materials. Adsorption Science & Technology 2022;2022. https://doi.org/10.1155/2022/3207986.

[149] Castells-Gil‡ J, Zhu‡ J, Itskou I, Wolpert EH, Hunter RD, Tidey JP, et al. Impact of N-heterocyclic amine modulators on the structure and thermal conversion of a zeolitic imidazole framework. J Mater Chem A Mater 2025;13:28006–18. https://doi.org/10.1039/D5TA04831A.

[150] Mirzanejad S, Bagherzadeh M, Bayrami A, Daneshgar H, Bahrami A, Mahdavi M. Improving the drug delivery performance of ZIF-8 with amine functionalization as a 5-fluorouracil nanocarrier. Sci Rep 2025;15:18793. https://doi.org/10.1038/s41598-025-03542-2.

[151] Butova V V., Polyakov VA, Budnyk AP, Aboraia AM, Bulanova EA, Guda AA, et al. Zn/Co ZIF family: MW synthesis, characterization and stability upon halogen sorption. Polyhedron 2018;154:457–64. https://doi.org/10.1016/j.poly.2018.08.006.

[152] Zhou K, Mousavi B, Luo Z, Phatanasri S, Chaemchuen S, Verpoort F. Characterization and properties of Zn/Co zeolitic imidazolate frameworks vs. ZIF-8 and ZIF-67. J Mater Chem A Mater 2017;5:952–7. https://doi.org/10.1039/C6TA07860E.

[153] Kaur G, Rai RK, Tyagi D, Yao X, Li P-Z, Yang X-C, et al. Room-temperature synthesis of bimetallic Co–Zn based zeolitic imidazolate frameworks in water for enhanced CO_2 and H_2 uptakes. J Mater Chem A Mater 2016;4:14932–8. https://doi.org/10.1039/C6TA04342A.

[154] Yao B, Lua S-K, Lim H-S, Zhang Q, Cui X, White TJ, et al. Rapid ultrasound-assisted synthesis of controllable Zn/Co-based zeolitic imidazolate framework nanoparticles for heterogeneous catalysis. Microporous and Mesoporous Materials 2021;314:110777. https://doi.org/10.1016/j.micromeso.2020.110777.

[155] Mor J, Nelliyil RB, Sharma SK. Fine-Tuning of the Pore Aperture and Framework Flexibility of Mixed-Metal (Zn/Co) Zeolitic Imidazolate Framework-8: An In Situ Positron Annihilation Lifetime Spectroscopy Study under CO_2 Gas Pressure. Langmuir 2023;39:10056–65. https://doi.org/10.1021/acs.langmuir.3c00996.

[156] Kümbetlioğlu F, Oskay KO, Çıplak Z, Ateş A. Preparation, Characterization, and Application of Metal Oxide-Doped Zeolitic Imidazolate Framework. ACS Omega 2023;8:27650–62. https://doi.org/10.1021/acsomega.3c03509.

[157] Ahmed Khalil S, Missaoui N, Alatawi RAS, Keshk AA, Alatawi O, Albalawi TA, et al. An Ultramicroporous Zinc-Based Zeolitic Imidazolate Framework-8 for the Adsorption of CO_2, CH_4, CO, N_2 and H_2: A Combined Experimental and Theoretical Study. ChemistrySelect 2024;9. https://doi.org/10.1002/slct.202402556.

[158] Rahman M, Kabir M, Islam T, Wang Y, Meng Q, Liu H, et al. Curcumin-Loaded ZIF-8 Nanomaterials: Exploring Drug Loading Efficiency and Biomedical Performance. ACS Omega 2025;10:3067–79. https://doi.org/10.1021/acsomega.4c09945.